WA-RD 84.1

TRAC

WASHINGTON STATE **TRA**NSPORTATION **C**ENTER

University of Washington

Washington State University

Washington State Department of Transportation

DETERMINATION OF THE CAPABILITY OF A SIDE BEARING BLOCK FOUNDATION AS A FIXED SUPPORT TO RESIST OVERTURNING

FILE COPY

By

Harold C. Sorensen, Ph.D. and Richard Toreh

Washington State Transportation Center

Structural Engineering Section
Department of Civil and Environmental Engineering
Washington State University
Pullman, Washington 99164-2914

Final Report

Research Project Y-2811
Task 21

Prepared for

Washington State Transportation Commission
Department of Transportation

and in cooperation with

U.S. Department of Transportation
Federal Highway Administration

May, 1986

TECHNICAL REPORT STANDARD TITLE PAGE

1. Report No.	2. Government Accession No.	3. Recipient's Catalog No.

4. Title and Subtitle	5. Report Date
Determination of the Capability of a Side Bearing Block Foundation as a Fixed Support to Resist Overturning	May, 1986
	6. Performing Organization Code
7. Author(s)	8. Performing Organization Report No.
Harold C. Sorensen and Richard Toreh	
9. Performing Organization Name and Address Structural Engineering Section Department of Civil and Environmental Engineering Washington State University Pullman, WA 99164-2914	10. Work Unit No.
	11. Contract or Grant No. Y-2811 Task No 21 Mod. No 2
12. Sponsoring Agency Name and Address Washington State Department of Transportation Transportation Building KF-01 Olympia, WA 98504-5201	13. Type of Report and Period Covered Final Report 6/84 - 5/86
	14. Sponsoring Agency Code

15. Supplementary Notes

Conducted in cooperation with the U.S. Department of Transportation, Federal Highway Administration

16. Abstract

A side bearing block foundation is used to resist overturning moments and lateral forces. Theoretical and experimental investigations were made to determine the ultimate moment capacity of a 3'x3'x7' reinforced concrete footing subjected to vertical and horizontal loads and an overturning moment.

The theoretical ultimate moment capacity was assumed to occur when the ultimate soil resistance was reached along the side bearing walls. It was found that the resultant friction force at the base of the foundation greatly influenced the capacity of the foundation to resist an overturning moment.

The experimental ultimate moment capacity was determined from a load-deflection curve obtained from field data.

A theoretical ultimate moment capacity was determined with the use of a finite element computer program.

The results from each of the three determinations were in acceptable agreement. Recommendations for further study are made.

17. Key Words	18. Distribution Statement
Footing, overturning, stability, soil mechanics, foundations, piles, finite element, soil pressure	

19. Security Classif. (of this report)	20. Security Classif. (of this page)	21. No. of Pages	22. Price
Unclassified		106	

Form DOT F 1700.7 (8-69)
HWY FORM 341-004 6/72

DISCLAIMER

The contents of this report reflect the views of the authors who are responsible for the facts and the accuracy of the data presented herein. The contents do not necessarily reflect the official views or policies of the Washington State Department of Transportation or the Federal Highway Administration. This report does not constitute a standard, specification or regulation.

TABLE OF CONTENTS

Page

LIST OF TABLES vi

LIST OF ILLUSTRATIONS vii

ACKNOWLEDGMENTS ix

ABSTRACT x

Chapter

1 INTRODUCTION 1

2 LITERATURE SEARCH 4

2.1 Lateral Load Bearing Piles 4

2.1.1 The "Pole" Theory or Rigid Pile Method 4

2.1.2 The Winkler Approach 6

2.1.3 Block Foundation Subject to Lateral Loads . . . 7

3 THEORETICAL DERIVATION OF PRELIMINARY EQUATIONS FOR THE DESIGN OF SIDE BEARING BLOCK FOUNDATIONS 13

3.1 General Considerations 13

3.2 General Theory for Soil Resistance of a Wall Section Subjected to an Overturning Moment and a Horizontal Force 14

3.3 Soil Pressures for a Side Bearing Block Foundation Subjected to an Overturning Moment and a Horizontal Force 21

3.3.1 Soil Pressures on a Prismatic Block Foundation . 21

3.3.2 Analysis for Soil Stresses at the Front and Rear Faces of the Foundation Which are Smaller than the Soil Pressures Based on Rankine's Theory 24

3.3.3 Analysis for the Soil Pressures Based on Rankine's Theory Reached Only at the Upper Part or at the Upper and Lower Parts of the Front and Rear Faces of the Foundation 24

3.4 Derivation of Preliminary Design Equations for Side Bearing Block Foundations 26

3.5 Application of the Preliminary Design Equations to the Test Foundation 33

3.6 Discussion 39

Page

Chapter

4 EXPERIMENTAL PROJECT 41
4.1 Background 41
4.2 Equipment and Test Foundation 41
4.3 Test Procedure 47
4.4 Test Results 51
4.4.1 Determination of the Ultimate Moment Resistance 58

5 COMPUTER PROGRAM 60
5.1 Discussion of the Model/Results 60

6 DISCUSSION AND COMPARISON 68

7 CONCLUSION AND RECOMMENDATIONS 71
7.1 Conclusion 71
7.1.1 Reliability of the Design Equations 71
7.1.2 Rotation Center 71
7.2 Recommendations 72
7.2.1 Field Test 73
7.2.2 Computer Program/Finite Element Formulation . . 73

REFERENCES 75

Appendix

A SOIL LAB TESTS AND APPLICATION OF THE DESIGN EQUATIONS . . 78

B CALCULATIONS OF THE MOMENTS AND LOADS ABOUT THE BASE OF THE FOUNDATION AND OF THE LOCATION OF THE ROTATION CENTER . . . 81

C STRAIN MEASUREMENTS AND COMPUTATIONS OF SOIL PRESSURES . . . 84

D DETERMINATION OF YIELD STRESSES 89

E ANSYS INPUT AND FINAL RESULTS 92

F DESIGN OF SIDE BEARING BLOCK FOUNDATIONS 100

LIST OF TABLES

Table		Page
1	The Maximum Moment, the Ultimate Moment Capacity and the Rotation Center for Soil Pressures Equal to One Times and Two Times the Values Based on the Rankine Theory	40
2	Loads Applied at Foundation from Load Box 1 (Step 2)	52
3	Loads Applied at Foundation from Load Box 1 and Load Box 2 (Step 3)	53
4	Location of the Rotation Center with Reference to the Applied Loads	56
5	Horizontal Movements of the Top of the Foundation	57
6	Values of the Ultimate Moment Capacity	68
7	Comparison of the Location of the Rotation Center	72
8	Readings and Soil Stresses	86

LIST OF ILLUSTRATIONS

Figure		Page
1	Resistance of a Laterally Loaded Pile	5
2	Soil Pressure Diagram for Side Bearing Block Foundations (Caquot/Kerisel)	8
3	Soil Pressure Diagrams for Side Bearing Block Foundations (Simpson/Edwards)	10
4	Rotation Center of Side Bearing Block Foundations	11
5	Side Bearing Wall Section	15
6	Pressure Diagram for Soil Pressures Smaller than Soil Pressures Based on Rankine's Theory, at All Points	16
7	Pressure Diagram for Soil Pressures Based on Rankine's Theory Only Induced at the Top of the Wall Section	16
8	Pressure Diagram for Soil Pressures Based on Rankine's Theory, Reached at the Upper and Lower Parts of the Wall Section	17
9	Maximum Soil Pressures: Pressure Diagram at Ultimate Soil Resistance	17
10	Pressure Diagram and (K_p - K_a) Diagram for Soil Pressures Based on Rankine's Theory Reached at the Upper and Lower Parts of the Wall Section	19
11	Side Bearing Block Foundation	21
12	Total Pressures at the Bearing Sides of the Block Foundation	22
13	Maximum Soil Pressures at the Side Bearing Walls	23
14	Soil Pressure Diagram for Soil Pressures Based on Rankine's Theory, Reached at the Top Only	25
15	Pressure Diagrams for Cohesive and Cohesionless Soils	27
16	Pressure Diagram for the Lower Part of the Block Foundation	29

Page

Figure

17 Pressure Diagram at the Ultimate Moment Capacity for Cohesionless Soils (Rotation Center at the Base of the Foundation) 32

18 Failure Wedge and Failure Planes 34

19 Test Foundation and Pressure Diagrams 36

20 Foundations and Leverarm Systems 43

21 Leverarm Systems 44

22 Strain Gage Boxes at the Side Bearing Walls 45

23 Strain Gage Boxes at the Bottom of the Foundation 46

24 Strain Gage Box 46

25 Four Arm Bridge Connection: Applied Circuit 48

26 Box with Rod, Pressure Face and Strain Gages 48

27 Horizontal and Vertical Movements of the Foundation 51

28 Rotation of the Block Foundation 55

29 Load - Deflection Curve 59

30 Finite Element Mesh 66

31 Location of Strain Gage Boxes at the Foundation 88

32 Linear Pressure Distribution 89

33 Average Soil Pressures Based on Rankine's Theory 91

34 Soil Pressure Diagram of the Block Foundation 103

ACKNOWLEDGMENTS

The authors express their sincere appreciation to the Washington State Department of Transportation in cooperation with the U.S. Department of Transportation, Federal Highway Administration for providing financial support for this project.

Appreciation is expressed to Mr. George Markich, Mr. Scott Rutherford and Mr. Bill Carr for their patience, counsel and advice during the conduct of the various research tasks.

The authors also wish to acknowledge the financial support given to this project by the Government of Indonesia and the Department of Civil and Environmental Engineering at Washington State University.

ABSTRACT

A side bearing block foundation is a system used to resist large overturning moments and/or lateral forces. The existing design equations for side bearing block foundations are not considered too reliable. An attempt is made to develop design equations, which are reasonably reliable and easy to use in practice. The sequence was as follows:

A) Derivation of preliminary design equations.

The ultimate moment capacity was assumed to occur when the ultimate soil resistance was reached along the side bearing walls. It was found that the resultant friction force at the base of the foundation affected to a great extent the capacity of the foundation to resist an overturning moment. To compare the results of the design equations to the data of a full-scale field test and to the results of an analysis performed by the finite element method, sample calculations were made.

B) Conducting a full-scale field test.

The test foundation was loaded by means of leverarms. Soil pressures were measured by the use of strain gages.

The ultimate moment capacity of the block foundation was approximated by using the load-deflection curve obtained from the field test.

C) An analysis, based on finite elements was made using a computer program.

Some of the assumptions were:

- a bilinear stress-strain curve for the soil elements with yield stresses according to the Rankine soil pressure theory.
- two dimensional interface elements.
- two dimensional isoparametric solid elements.

The results of the computed rotation center compared well to that obtained by the field test and the finite element program.

It was found that a "correction factor" of 2½ (for the lateral earth pressures based on Rankine's theory) was required to be used in the design equations. This correction factor is only valid for the dimensions used for the test foundation. The factors affecting the magnitude of the "correction factors" are discussed.

For the design of side bearing block foundations, the design loads and the allowable deflection are discussed in a sample computation (Appendix F).

Recommendations for further study are made.

CHAPTER 1

INTRODUCTION

The resistance of a foundation system against lateral loads and/or moments is of importance to the design of fixed supports. For the design of foundations subjected to large lateral loads and/or moments two systems exist:

1. Pile foundations
2. Block foundations

During the last one hundred years, many experiments and tests were conducted (26, 14 and others) and a variety of methods of analyses and design of piles subjected to lateral loads were proposed, but the design of piles subjected to lateral loads is still a matter of concern.

Based on large-scale tests conducted in France, Sweden and Great Britain, empirical formulas and tables were developed for the design of side bearing block foundations against lateral loads and/or overturning moments. Those formulas and tables for many types of soils were based on an assumed rotation center at the base of the foundation (6) or at an assumed fixed point above the base (28, 31).

A rigorous solution for the design of a side bearing block foundation is very complex. The solution to the problem is rigorous if the computed stresses are perfectly compatible with the conditions of equilibrium, the boundary conditions, and the assumed mechanical properties of the material. However, it is necessary to develop a "theoretical" solution based on acceptable assumptions, to find practical methods to solve the problem by modifications and simplifications and to develop design equations involving "simple calculations" for side bearing

block foundations which are sufficiently reliable and practical. The mechanical response of a soil is affected by its material characteristics. The stress-strain characteristics of a soil are very complex; those characteristics are nonlinearity, time dependency, dependency on the magnitudes of the stresses in the soil, anisotropicity, and others. Furthermore, the characteristics are affected by a variety of factors, i.e., stress history, soil moisture, and permeability. Thus it becomes necessary to idealize the behavior of the soil by adopting some arbitrary simplifications and to represent the stress-strain characteristics in a reasonable way to achieve a practical approximation.

The intention of the present study is to develop a "theoretical" practical solution and to derive practical design equations for side bearing block foundations. The approach is as follows:

A. A theoretical derivation of preliminary equations based on some simplifying assumptions.

B. Experimental project: conducting a full-scale field test to obtain data on the ultimate moment capacity of a laterally loaded block foundation.

C. Application of a finite element approach using a computer program in order to compare to the results obtained in A and B. Values of the soil parameters were obtained from simple lab tests and utilized in the input of the ANSYS computer program.

For an evaluation of the reliability of the equations developed in A, the results of B and C are needed. The results of the comparison and the combined analysis are incorporated in a final set of design equations.

As only one field test was conducted and a two-dimensional assumption in the computer program was applied, more field tests and a three-dimensional computer program will probably be needed to obtain a more refined and reliable solution to the foundation problem. The present work is therefore seen as an initial step in providing insight into the failure mechanism for the block foundation and as a base for studies of a more readily applicable nature.

CHAPTER 2

LITERATURE SEARCH

The design of foundations subjected to lateral loads and/or large moments has been the subject of various investigations and studies for more than a century. Although literature and data presently available for the design of lateral load resisting block foundations are scarce, literature on lateral load resisting piles is numerous. As similarities exist between lateral load bearing piles and side bearing block foundations, some related data and assumptions valid for the analysis of piles are useful in the analyses of side bearing block foundations.

2.1 Lateral Load Bearing Piles

The earliest experiments (Sandeman in 1880 and others) provided data for the design of laterally loaded piles. As a result of those tests, empirical formulas were derived and became available (12, 14 and others), but the danger based on limited data was realized, and large safety factors were used for the allowable loads on piles.

2.1.1 The "Pole" Theory or Rigid Pile Method

The "Pole" theory (36) subsequently improved upon and most favored by practicing engineers, assumes an absolutely rigid pole pivoting about a point along its length (36). Czerniak (8) assumed that before the passive pressure is reached, the earth mass is in an elastic state. Referring to Fig. 1, the unit resistance $R_y = \frac{Wy}{L}$, as the soil resistance is assumed to increase proportionately with depth. Since $\Delta_y = \frac{(r - y)}{r} \Delta$ (Fig. 1a), and $P_y = \Delta_y \frac{Wy}{L}$, the pressure diagram is parabolic (Fig. 1c).

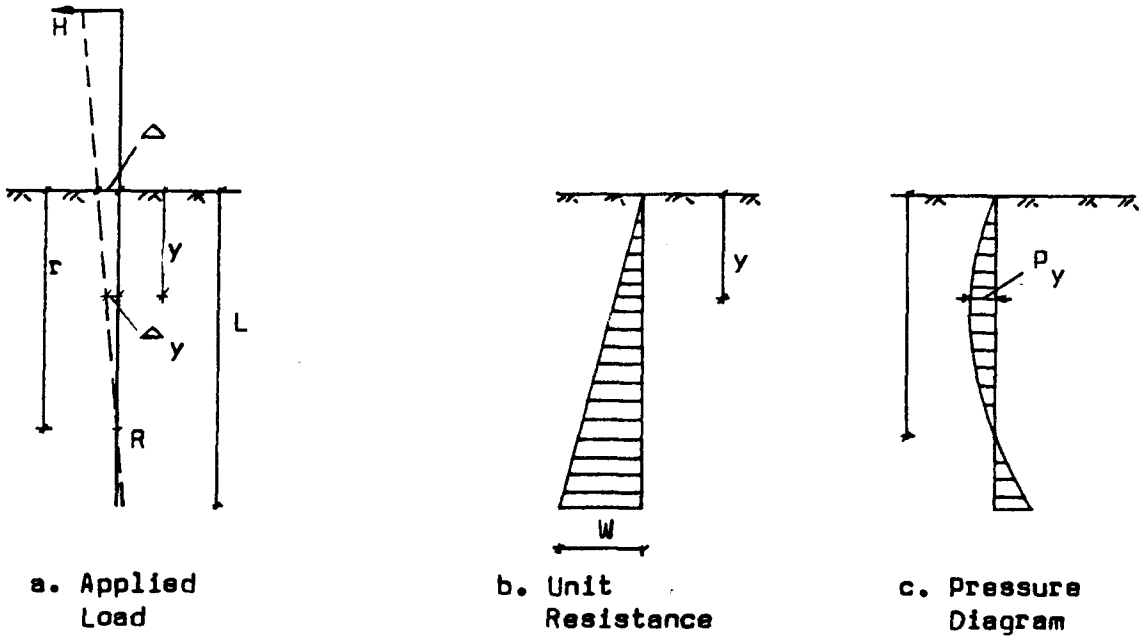

Figure 1. Resistance of a Laterally Loaded Pile

By differentiating P_y with respect to y the maximum pressure at r/2 is obtained. The other maximum value occurs at depth y = L. By setting each of the maximum values equal to the allowable pressure, two values are obtained for L (Fig. 1a). The value for L obtained by setting the allowable pressure equal to the maximum pressure at r/2 governs the design. Czerniak (8) obtained the allowable pressure from a building code table, while Downs (10) assumed the "allowable" pressure to be the passive soil pressure based on Rankine's theory at y = r/2 and y = L, respectively.

Broms (4) classified the piles as:

A. Short piles

B. Intermediate piles

C. Long piles

The classification is based on the dimensionless quantity nL, in which n is equal to $(n_h/EI)^{1/5}$ and n_h is the coefficient of horizontal subgrade reaction (5). Broms classified a pile as short if nL is less than 2 and as long if nL exceeds 4. For single piles, the modulus of subgrade reaction k was used for the computation of the lateral deflections at working loads. For the ultimate lateral resistance, it was assumed that the ultimate resistance was reached when the "full lateral resistance of the soil" develops along the total length of the pile (or when the yield strength of the pile section is reached). For short piles it was assumed that the ultimate lateral resistance was governed by the lateral resistance of the soil, and that the rotation center was at the bottom. For single short piles the maximum lateral earth pressure at failure was assumed to be three times the passive earth pressure based on Rankine's theory for a cohesionless soil. The reason for this assumption is based on the observations made by Prakash (25).

2.1.2 The Winkler Approach

The Winkler method, proposed by E. Winkler in 1867, is in some ways similar to the "pole theory," but it treats the soil mass at the side bearing "walls" of the piles as a series of springs:

A. The springs are independent of each other, i.e., no interaction exists between the springs.

B. The soil is assumed to be linearly elastic for the calculation of the ultimate resistance against lateral loads.

The Winkler hypothesis states that the contact pressure P at a point is proportional to the displacement W of that point, i.e., P = kW, in which k is the modulus of subgrade reaction (2, 29). This linear elastic behavior is widely used in soil-foundation interaction problems, although it is a difficult task to establish a realistic value of the modulus of subgrade reaction of a soil (11).

Bowles (2) developed a computer program using the Winkler approach and the finite element method in which the friction at the walls and the stresses at the base of the pile are neglected.

The finite difference method has been applied by several authors, although in practice, people were skeptical of this analytical method.

The present methods used in the design of piles subjected to lateral loads are considered relatively inaccurate and large safety factors are used for the allowable lateral loads on piles (16).

2.1.3 Block Foundation Subject to Lateral Loads

No reliable and accurate methods are available for the design and analysis of side bearing block foundations. In some handbooks, standards are given as guides in the design of block foundations subject to lateral loads. Those standards are based on experience (6, 28, 31).

Caquot/Kerisel (6) discussed a practical French method, used by "Die Technishe Kommission des Syndicat Professionel des Producteurs und Distributeurs d'Energie Electrique" (Fig. 2).

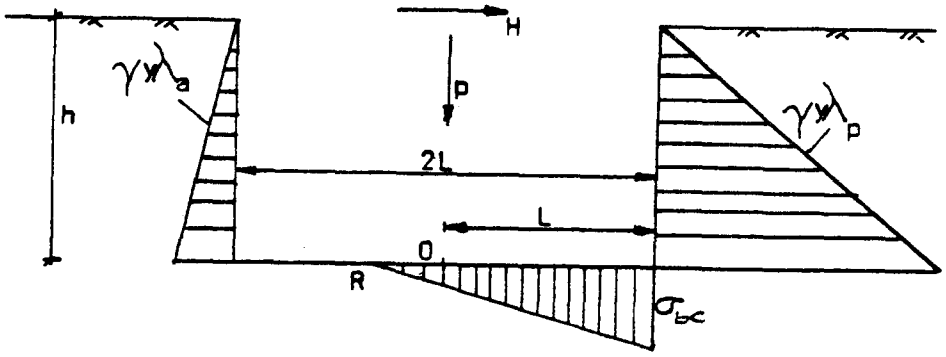

Figure 2. Soil Pressure Diagrams for Side Bearing Block Foundations (Caquot/Kerisel)

This French method assumes that at the ultimate moment resistance, earth pressures $P_a = \gamma\ y\ \tan^2\ (45 - \frac{\phi}{2})$ and $P_p = \gamma\ y\ \tan^2\ (45 + \frac{\phi}{2})$ are developed at the rear wall and front wall, respectively. It was also assumed that at the utmost front of the base, the soil stress was equal to the ultimate bearing capacity σ_{bc} of the soil.

For $\lambda_a = \tan^2\ (45 - \frac{\phi}{2})$; $\lambda_p = \tan^2\ (45 + \frac{\phi}{2})$

b = the width of the foundation perpendicular to the plane of the figure

$$\mu = (1 - \frac{2}{3}\frac{P}{\sigma_{bc} bL}) \qquad \nu = (\frac{\lambda_p - \lambda_a}{6\sigma_{bc}})$$

M_r = ultimate moment resistance with respect to 0

M'_r = moment resistance of the soil pressures at the base with respect to 0

M''_r = moment resistance of the lateral soil pressures at the side bearing walls with respect to 0

$$M'_r = P(L - \frac{x}{3}) = P(L - \frac{2}{3}\frac{P}{\sigma_{bc} b})$$

$$M''_r = b\,\frac{h}{3}\left(\tfrac{1}{2}\,\gamma\,h^2\,\lambda_p - \tfrac{1}{2}\,\gamma\,h^2\,\lambda_a\right)$$

$$M_r = M'_r + M''_r = P\left(L - \frac{2}{3}\,\frac{P}{\sigma_{bc}b}\right) + \frac{bh^3}{6\sigma_{bc}}\,(\lambda_p - \lambda_a)$$

By expanding and collecting terms

$$M_r = \mu PL + \nu\gamma bh^3$$

It can be concluded that:

1. The point of rotation is assumed to be at the base (point R).
2. The friction is neglected.

The values for five different soils, based on data from tests on transmission tower foundations, were presented by "the Kommission" in tabulated form. (Note: this method is similar to that of Seelye (28), but Seelye assumed that the rotation center was at a depth of 2h/3 at the rear wall of the foundation).

For shallow concrete block foundations subjected to lateral loads Simpson and Edwards (31) used formulas valid for the analysis of wood poles in Great Britain (Fig. 3). Two different assumptions which evolved from experience in "all types of soils" are as follows:

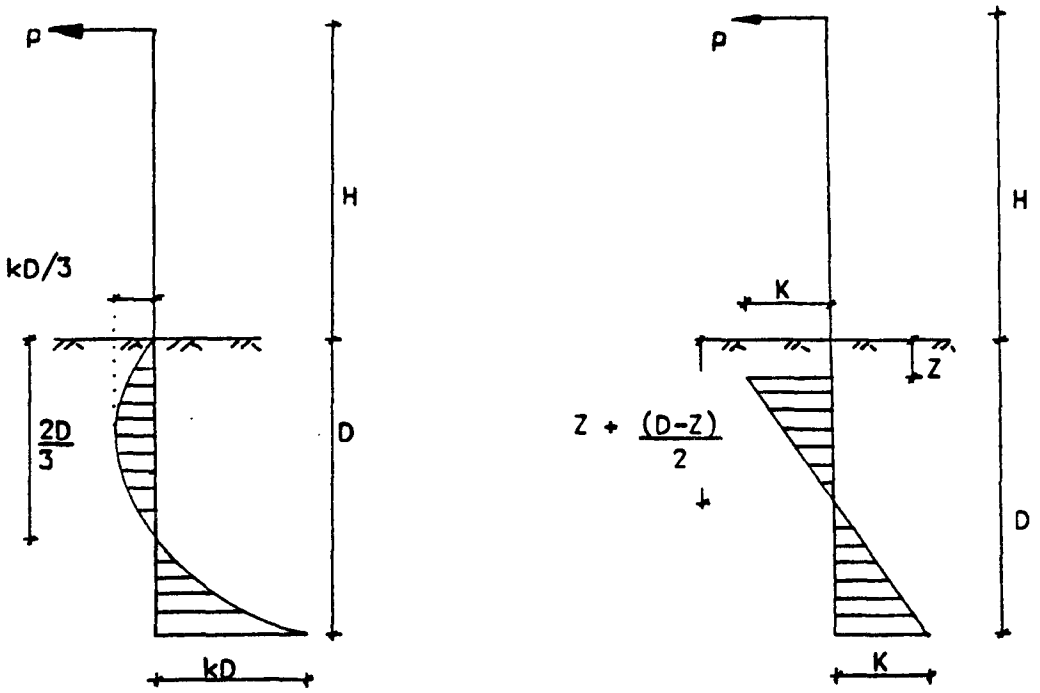

Figure 3. Soil Pressure Diagrams for Side Bearing Foundations (Simpson/Edwards)

b = width of the block foundation perpendicular to the plane of the figure

k and K are constants based on experience

D = embedded depth

Z = amount of soil neglected (at least one foot)

In Fig. 3a, it was assumed that the soil resistance per unit deflection increases proportionately with depth. The stress distribution is parabolic, and b or D has to be assumed to solve the equation:

$$P(H + \frac{2D}{3}) = kbD^3/12$$

In Fig. 3b, a constant soil resistance per unit deflection is assumed. The stress distribution is linear and

$$P(H + z + \frac{(D - Z)}{2}) = Kb \frac{(D - Z)^2}{6}$$

Note: The moment resistance due to the soil reaction at the bottom of the foundation has been neglected (and d = breadth of the foundation has not been mentioned).

Friction forces at the base are neglected.

The points of rotation are assumed to be fixed as shown in the figures.

From the above discussion it can be concluded that a more exact solution is possible. For the side bearing block foundations, Caquot/Kerisel (6) suggested that "the determination of a temporary rotation center" C (Fig. 4) would be the basis of an exact solution, and that tests in Sweden proved that the location of the rotation center depended on "the nature" of the soil and the force-system.

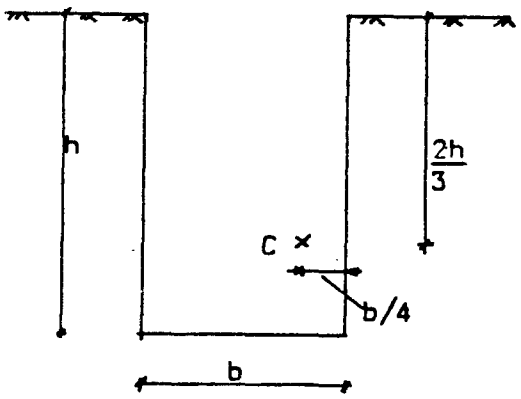

Figure 4. Rotation Center of Side Bearing Block Foundations

Caquot/Kerisel also mentioned that the tests by the "Association Suisse des Electriciens" showed that the rotation center was generally at C, i.e., at a depth (2/3)h and at a distance of (1/4)b from the "compressed" side (Fig. 4). However, no practical solution was developed.

CHAPTER 3

THEORETICAL DERIVATION OF PRELIMINARY EQUATIONS FOR THE DESIGN OF SIDE BEARING BLOCK FOUNDATIONS

3.1 General Considerations

In the following, an attempt is made to derive practical solutions for the design of side bearing block foundations which will not involve complicated computations.

Some significant data and assumptions "valid" for the analysis of side bearing piles will be used for guidance and utilized in the derivation of the preliminary solutions for the design and analysis of the block foundations.

Terzaghi (33) observed from tests on large retaining walls that, after the walls have moved beyond a certain critical distance, the distribution of the lateral pressure in sand is always hydrostatic. Therefore, for the analysis, active and passive lateral earth pressures based on Rankine's theory are adopted for the values of the maximum earth pressures. This method assumes that no friction exists between the soil and vertical faces of the foundation. If, for a vertical face and a horizontal ground surface an error exists because of this assumption, the error will be made on the safe side (27).

The following items will be discussed in order.

A. General theory for soil resistance of a wall section subjected to an overturning moment and a horizontal force.

B. Soil pressures for a side bearing block foundation subjected to an overturning moment and a horizontal force.

C. Derivation of preliminary design equations for side bearing block foundations.

D. Applications of the preliminary design equations to the test foundation.

In this report at the end of most of the sections, soils with cohesion will also be discussed.

3.2 General Theory for Soil Resistance of a Wall Section Subjected to an Overturning Moment and a Horizontal Force

Rankine's pressures:

$$P_p = \gamma y \tan^2(45 + \frac{\phi}{2}) = \gamma y K_p$$

$$P_a = \gamma y \tan^2(45 - \frac{\phi}{2}) = \gamma \frac{y}{a} K_a \qquad (3.1)$$

Consider a wall section with the following data given (Fig. 5):

embedded height = L

width (perpendicular to the plan of figure) = 1 unit

thickness t = very small

stiffness = infinite

depth of rotation center = Y_{rc}

For small values of H and M, the wall section rotates about point R, but the soil pressures at the front vertical face and at the rear vertical face will be smaller than P_p and P_a (at all points). For greater values of the overturning moment, P_p and P_a are induced at the top points E and F; and for successively greater values of the overturning moment, P_p and P_a will also be reached at lower and lower points. The same is true for points below the rotation point R where P_p and P_a will first be reached

at the lowest points B and A and then successively at higher and higher points. If P_a is superimposed onto P_p, the results are the pressure diagrams as shown in Figs. 6, 7, 8 and 9.

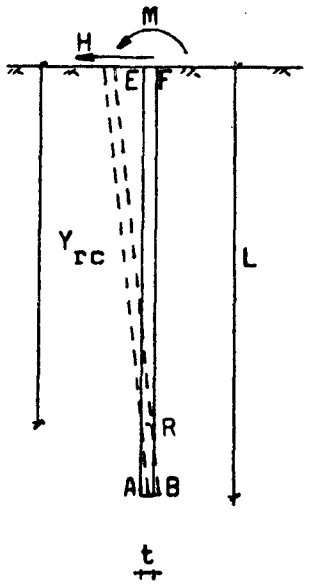

Figure 5. Side Bearing Wall Section

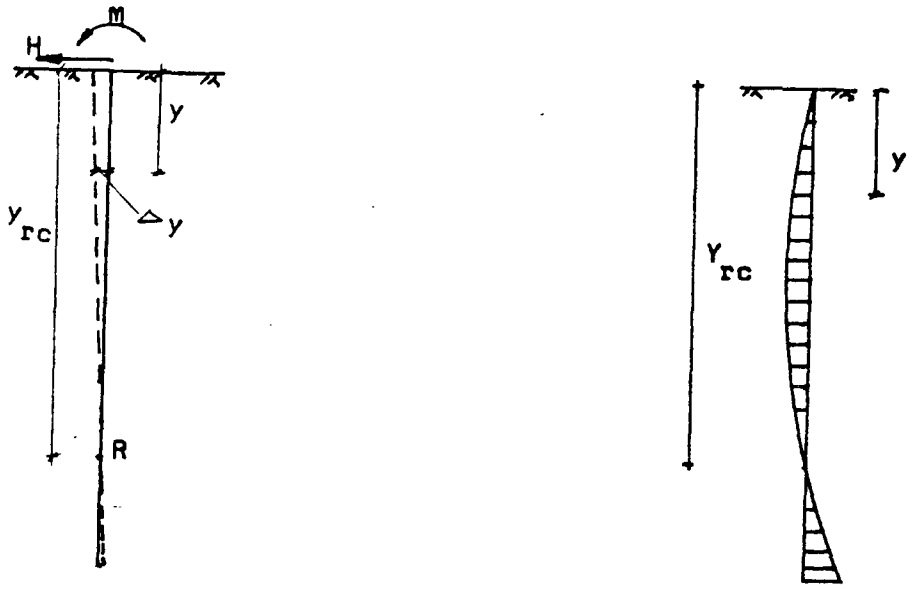

Figure 6. Pressure Diagram for Soil Pressures Smaller than Soil Pressures Based on Rankine's Theory, at All Points

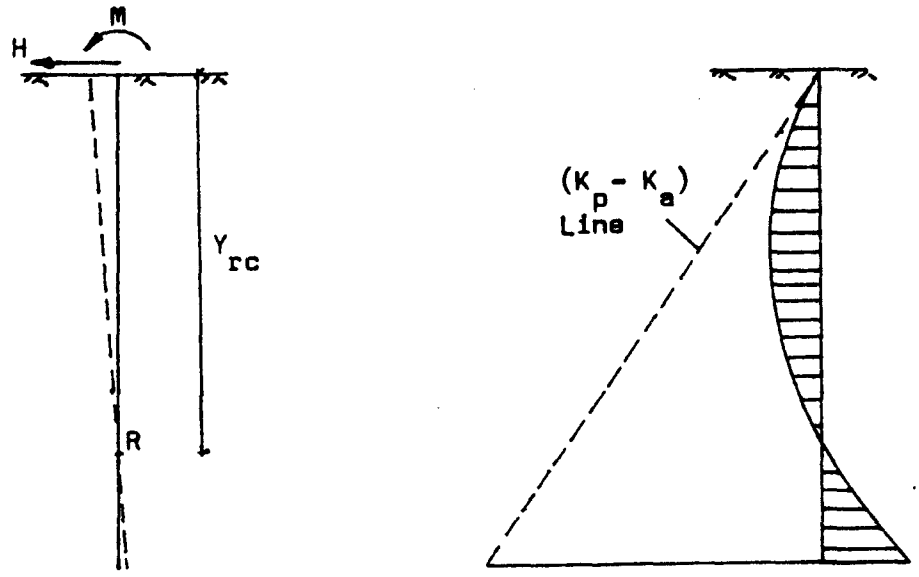

Figure 7. Pressure Diagram for Soil Pressures Based on Rankine's Theory Only Induced at the Top of the Wall Section

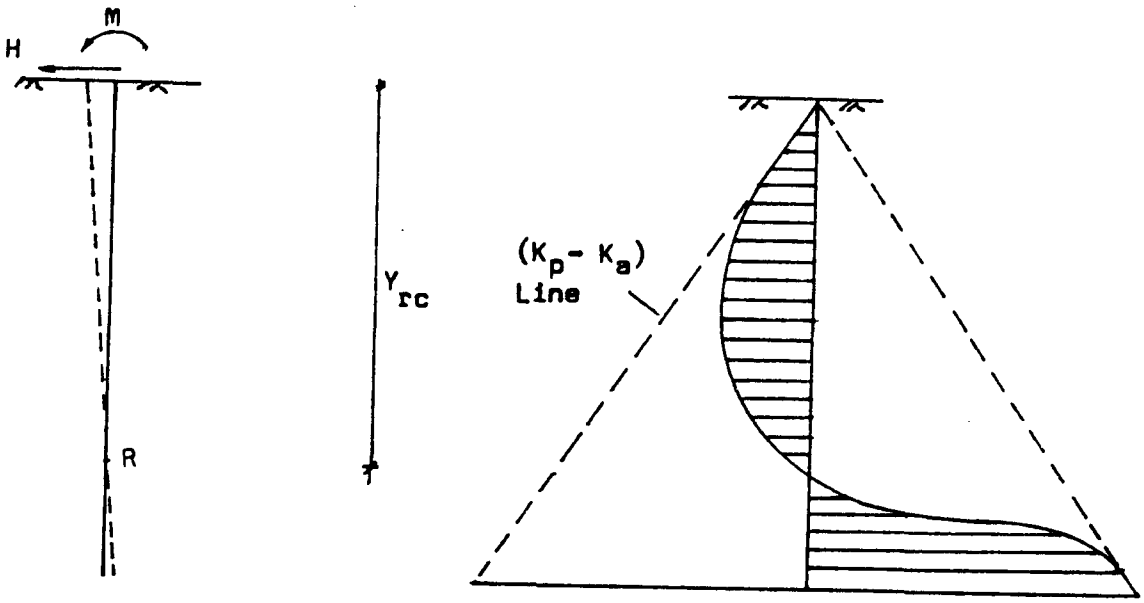

Figure 8. Pressure Diagram for Soil Pressures Based on Rankine's Theory, Reached at the Upper and Lower Parts of the Wall Section

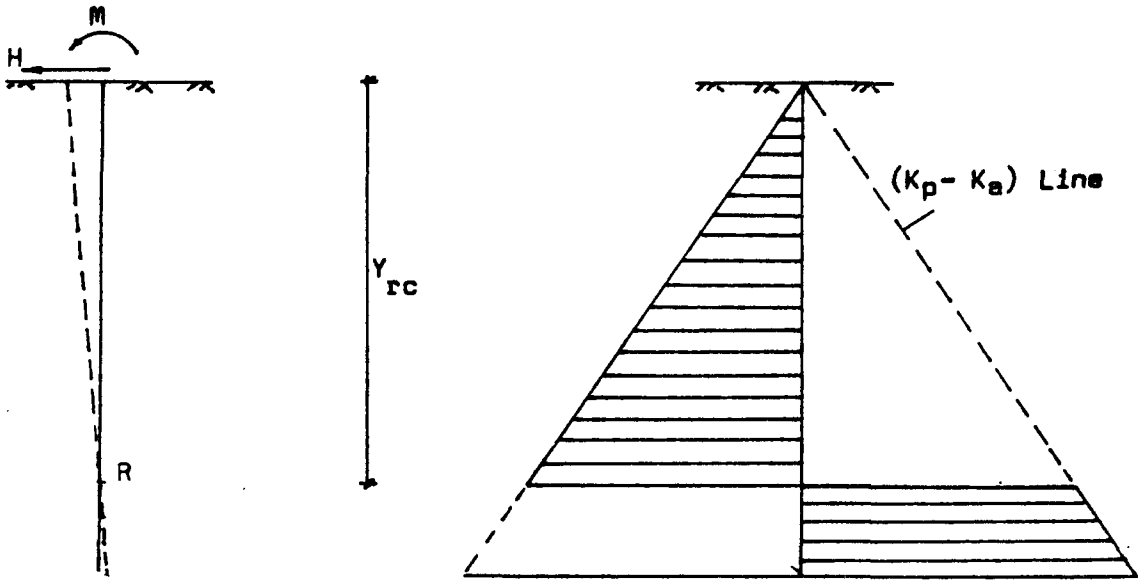

Figure 9. Maximum Soil Pressures: Pressure Diagram at Ultimate Soil Resistance

In Fig. 6, where all the soil pressures are smaller than the pressures based on Rankine's theory, the state of pressure is elastic and the stress is proportional to the deflection. The pressure diagram is parabolic for cohesionless soils, and the rotation and pressure diagram can be computed by the "pole theory" using the soil modulus (modulus of subgrade reaction)

$$K_s = A_s + B_s\, y^n \quad (2)$$

A_s and B_s can be evaluated by tests. Approximate values are given by Broms (4) for cohesive and cohesionless soil. For cohesionless soils $A_s = 0$ and $n = 1$ (2 and 4). By assuming the rotation center (Fig. 1) to be at a depth Y_{rc}, and the deflection at the top = Δ, the horizontal displacement (if the "pole" is absolutely rigid") at depth y is:

$$\Delta_y = \left(\frac{Y_{rc} - y}{Y_{rc}}\right) \Delta$$

and the horizontal pressure at depth y is:

$$\sigma_y = \Delta_y\, k_s$$

By the equations of static equilibrium: $\Sigma F_x = 0$ and $\Sigma M = 0$, the rotation center and the rotation can be found.

In Fig. 7, where the soil pressures based on Rankine's theory are reached only at the top of the wall, the pressure diagram can be computed by the method used for the calculations of the pressure diagram of Fig. 8 as follows.

In Fig. 8, where the soil pressures based on Rankine's theory are reached at the upper and lower parts of the wall section, the pressure diagram will be computed as follows (Fig. 10):

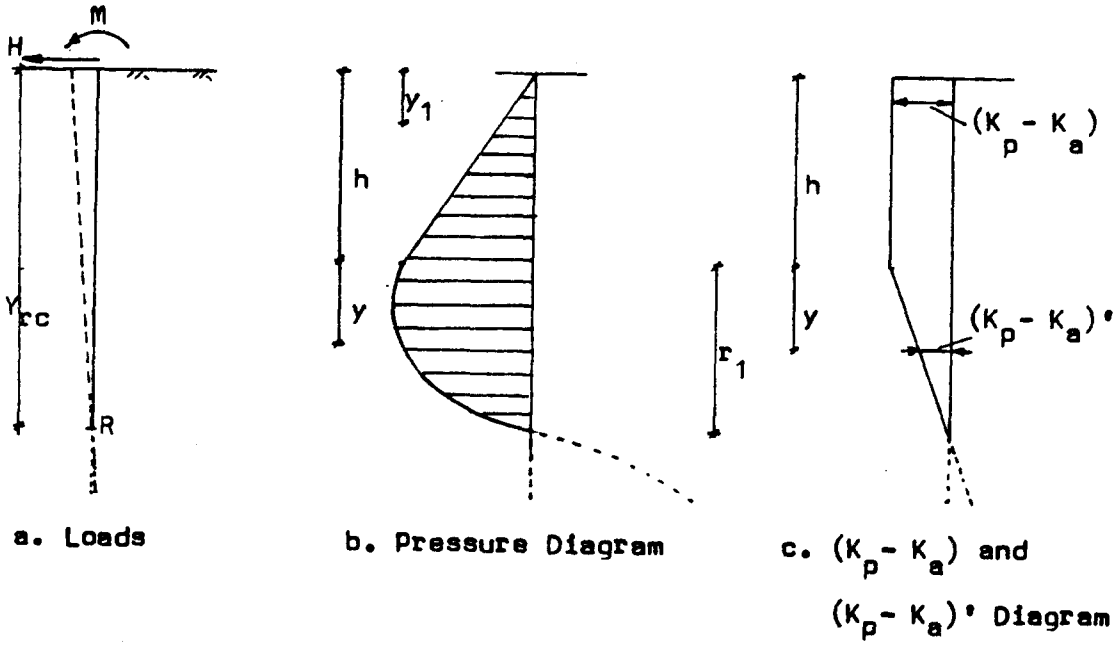

Figure 10. Pressure Diagram and $(K_p - K_a)$ Diagram for Soil Pressures Based on Rankine's Theory Reached at the Upper and Lower Parts of the Wall Section

The stresses based on Rankine's theory are reached at the top part and the value of the soil at depth y_1 is: $P_{y1} = \gamma y_1(K_p - K_a)$ for $0 < y_1 < h$. For depths greater than h, the soil pressures will be smaller than $\gamma(h + y)(K_p - K_a)$ and are equal to $\gamma(H + y)(K_p - K_a)'$ (Fig. 10c). The value of $(K_p - K_a)'$ can be computed from Fig. 10c:

$$(K_p - K_a)' = \left(\frac{r_1 - y}{r_1}\right)(K_p - K_a) = \left(\frac{r_1 - y}{r_1}\right)\left(\tan^2\left[45 + \frac{\phi}{2}\right] - \tan^2\left[45 - \frac{\phi}{2}\right]\right)$$

and the soil pressure at depth $(h + y)$ is:

$$P_{(h + y)} = \gamma(h + y)\left(\frac{r_1 - y}{r_1}\right)(K_p - K_a)$$

This is a second order curve (Fig. 10b) and for $y = r_1$ the pressure is equal to zero (for a depth Y_{rc} from the surface).

The case shown in Fig. 7 is for $h = 0$, where the soil pressure based on Rankine's theory is only induced at the top, and where

$$P_y = \gamma y \left(\frac{Y_{rc} - y}{Y_{rc}}\right) (K_p - K_a)$$

For the case shown in Fig. 9, the pressure diagrams for the parts above and below the rotation point R, are both following the $(K_p - K_a)$ lines. This is a "theoretical" pressure diagram, since in reality the deflection very near point R cannot be so great as to induce the pressures predicted by Rankine's theory. The ultimate soil resistance and the ultimate moment capacity is easily computable. For a known horizontal force H, Y_{rc} and M (Fig. 9) can be solved by applying $\Sigma M = 0$ and $\Sigma F_H = 0$. The foundation will theoretically not be able to sustain a moment greater than the ultimate.

3.3 Soil Pressures for a Side Bearing Block Foundation Subjected to an Overturning Moment and a Horizontal Force

3.3.1 Soil Pressures on a Prismatic Block Foundation

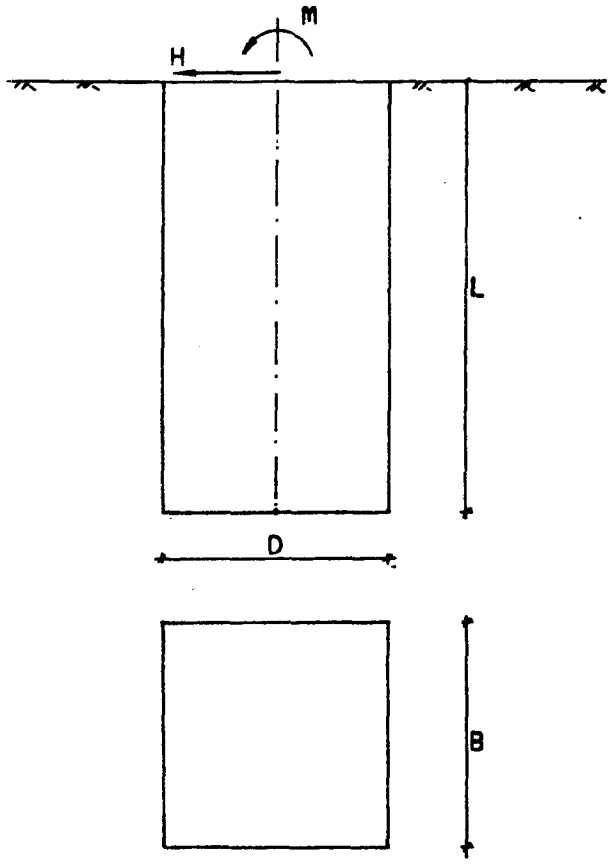

Figure 11. Side Bearing Block Foundation

For the value of the ultimate lateral resistance, the pressures based on Rankine's theory have been assumed. In Section 3.1 it was indicated that this includes the assumption that no friction exists between the front and rear faces of the foundation and the soil. The pressure diagrams for an increasing overturning moment are illustrated in Figs. 12a, b, c and Fig. 13.

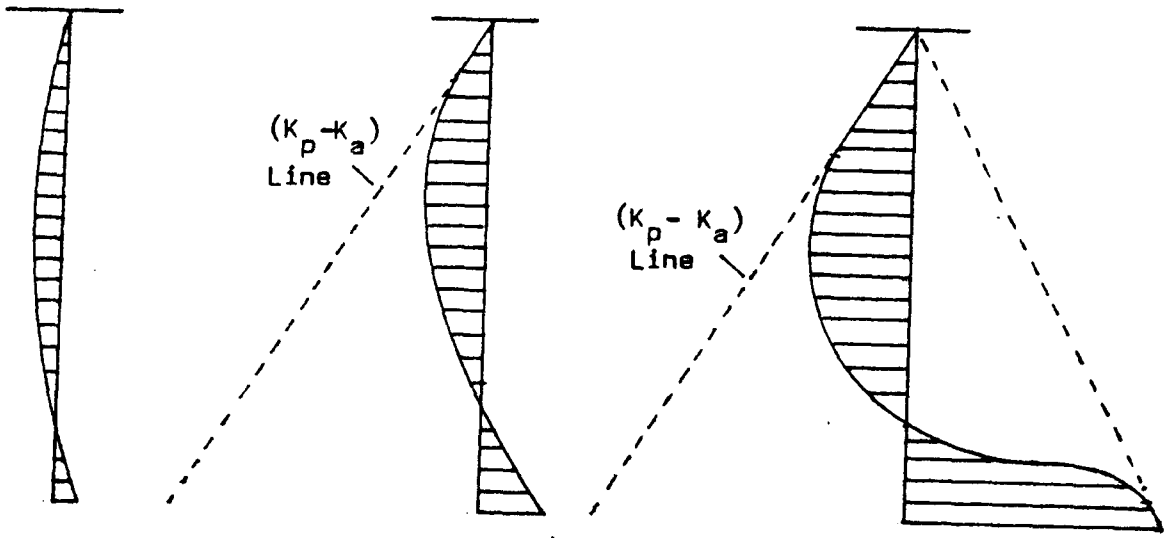

a. All Soil Pressures Smaller than the Soil Stresses Based on Rankine's Theory

b. Soil Pressures Based on Rankine's Theory Reached at the Upper Part Only

c. Soil Pressures Based on Rankine's Theory Reached at the Upper and Lower Part

Figure 12. Total Pressures at the Bearing Sides of the Block Foundation

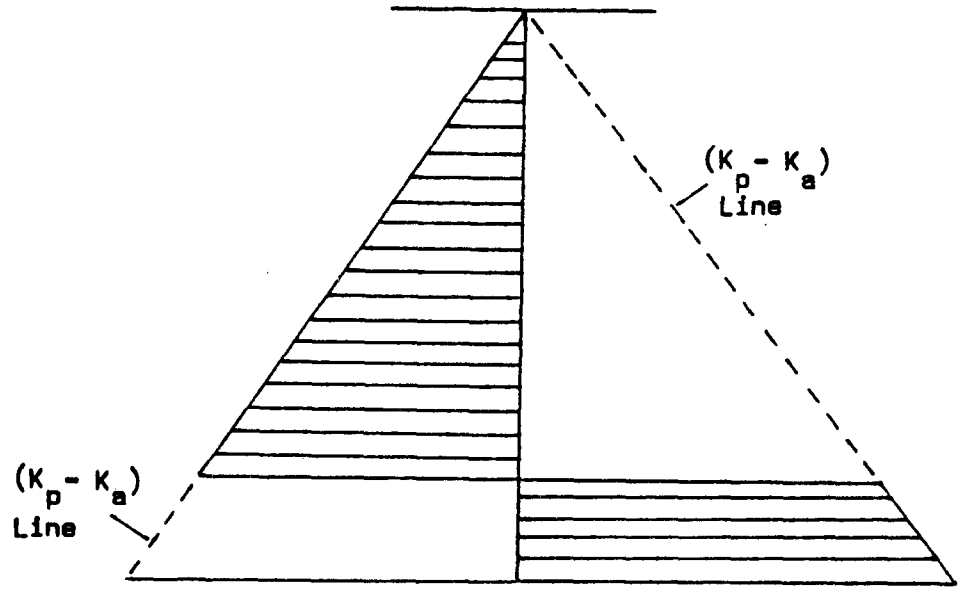

Figure 13. Maximum Soil Pressures at the Side Bearing Walls

A. In Fig. 12a, the overturning moment is so small that the soil pressures along the vertical front and rear faces are all smaller than the soil pressures based on Rankine's theory.

B. In Fig. 12b and Fig. 12c, the overturning moment is larger, such that the "maximum" soil pressures are reached at the upper part only, or at the upper and lower parts of the front and rear faces of the foundation.

C. In Fig. 13, at the ultimate moment capacity, the soil pressures at the front and rear faces are equal to the soil pressures based on Rankine's theory along the total depth of the block foundation.

For all three cases, the friction between the soil and the walls perpendicular to the side bearing walls has been neglected.

3.3.2 Analysis for Soil Stresses at the Front and Rear Faces of the Foundation Which are Smaller than the Soil Pressures Based on Rankine's Theory (Fig. 12a)

The soil pressures at the front and rear vertical faces can be computed, as the state of stress can be assumed to be the elastic state. The "pole theory" can be used to compute the parabolic stress diagram (see Section 3.2) and the rotation.

3.3.3 Analysis for the Soil Pressures Based on Rankine's Theory Reached Only at the Upper Part or at the Upper and Lower Parts of the Front and Rear Faces of the Foundation (Figs. 12b and c)

The soil pressures in this case do not give the ultimate moment capacity of the foundation. However, the case in Fig. 12b will be analyzed here, and the resultant horizontal soil pressures with their lines of action computed.

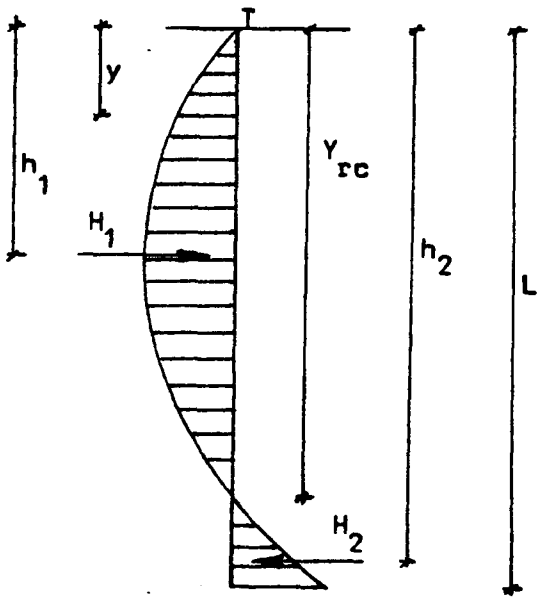

Figure 14. Soil Pressure Diagram for Soil Pressures Based on Rankine's Theory, Reached at the Top Only

For simplicity, the case where the soil pressure based on Rankine's theory is reached only at the top point T of the rear and front wall (Fig. 14) is considered.

From Section 3.2:

$$P_y = \gamma y\left(\frac{Y_{rc} - y}{Y_{rc}}\right)(K_p - K_a)$$

$$H_1 = \int_0^{Y_{rc}} P_y\, dy = \gamma(K_p - K_a) \int_0^{Y_{rc}} y\left(\frac{Y_{rc} - y}{Y_{rc}}\right) dy$$

$$H_1 = \gamma(K_p - K_a)\left(\frac{y^2}{2} - \frac{y^3}{3Y_{rc}}\right)\Bigg|_0^{Y_{rc}} = \gamma(K_p - K_a)\frac{Y_{rc}^2}{6}$$

H_1 acts at depth h_1

$$H_1 h_1 = \int_0^{Y_{rc}} P_y \, y dy = \gamma(K_p - K_a) \int_0^{Y_{rc}} y\left(\frac{Y_{rc} - y}{Y_{rc}}\right) y dy$$

$$= \gamma(K_p - K_a) \left(\frac{y^3}{3} - \frac{y^4}{4Y_{rc}}\right) \Bigg|_0^{Y_{rc}} = \gamma(K_p - K_a) \frac{Y_{rc}^3}{12}$$

$$h_1 = \frac{Y_{rc}}{2}$$

and

$$H_2 = -\gamma(K_p - K_a) \int_{Y_{rc}}^{L} y\left(\frac{y - Y_{rc}}{Y_{rc}}\right) dy = -\gamma(K_p - K_a) \left(\frac{L^3}{3Y_{rc}} - \frac{L^2}{2} + \frac{Y_{rc}^2}{6}\right)$$

$$H_2 h_2 = -\gamma(K_p - K_a) \int_{Y_{rc}}^{L} y^2\left(\frac{y - Y_{rc}}{Y_{rc}}\right) dy = -\gamma(K_p - K_a)\left(\frac{L^4}{4Y_{rc}} - \frac{L^3}{3} + \frac{Y_{rc}^3}{12}\right)$$

$$h_2 = \frac{\left(\frac{L^4}{4Y_{rc}} - \frac{L^3}{3} + \frac{Y_{rc}^3}{12}\right)}{\frac{L^3}{3Y_{rc}} - \frac{L^2}{2} + \frac{Y_{rc}^2}{6}}$$

Y_{rc} can be obtained from $\Sigma H = 0$.

Similarly, H_1, h_1, H_2 and h_2 can be computed for the pressure diagrams in Figs. 12b and c (see Section 3.1).

3.4 Derivation of Preliminary Design Equations for Side Bearing Block Foundations

At the ultimate loads, the soil pressures at the front and rear faces are equal to the soil pressures based on Rankine's theory along the total depth of the block foundation (Fig. 13).

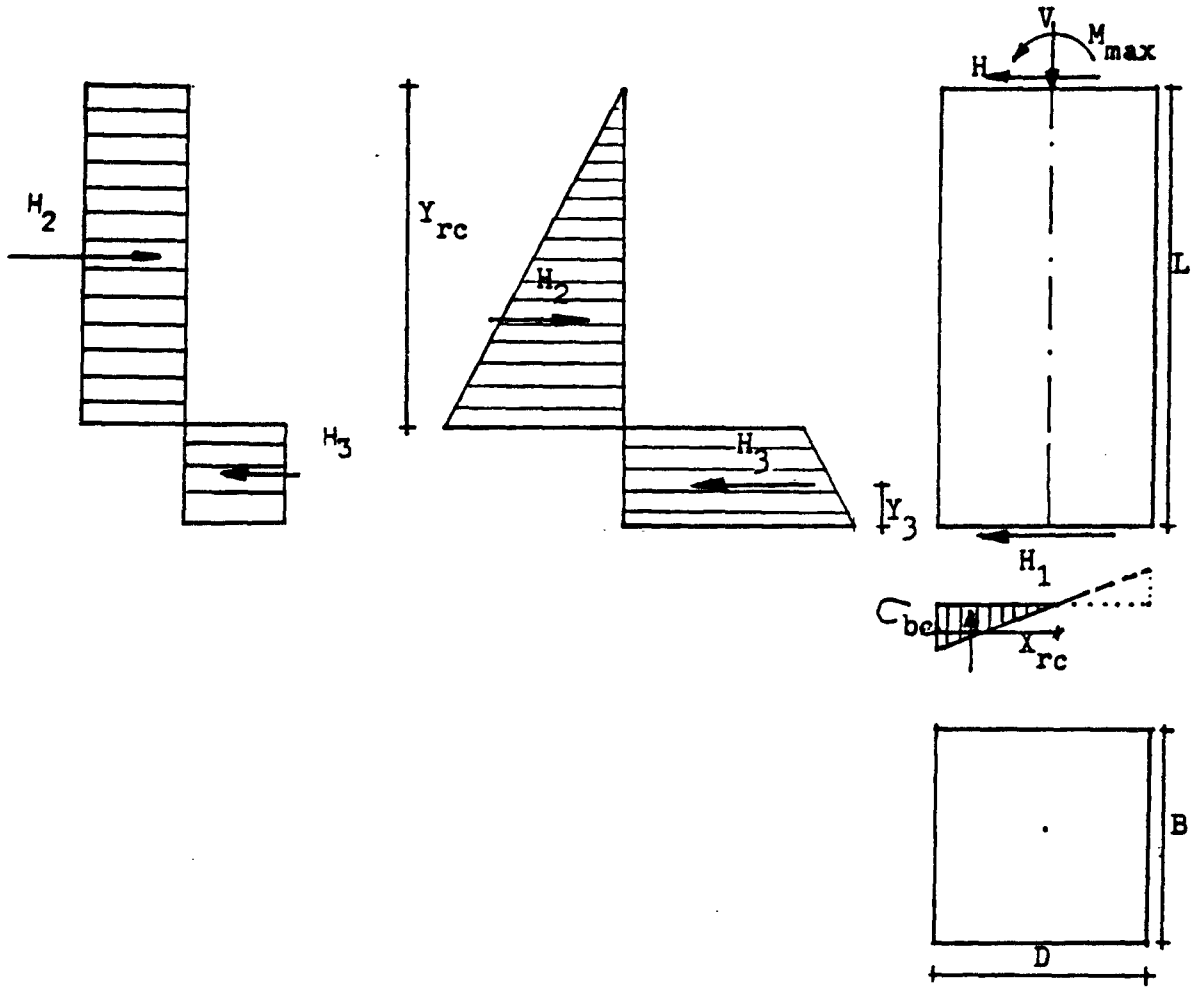

a. Pressure Diagram for Cohesive Soils

b. Pressure Diagram for Cohesionless Soils

c. Vertical Pressure Diagram for Cohesionless and Cohesive Soils

Figure 15. Pressure Diagrams for Cohesive and Cohesionless Soils

For side bearing block foundations, the pressure diagram shown in Fig. 15b is generally used for cohesionless soils and the pressure diagram shown in Fig. 15a is generally used for cohesive soils. (The application of the loads is generally "quick," causing excess pore

pressures. This means an "undrained" soil resistance.) The friction forces at all the walls are again neglected, but the friction force H_1 at the bottom is important in the determination of the rotation center.

μ = coefficient of friction at the base of the foundation.

V_{tot} = total vertical load

H_1 will have a maximum value:

$$H_{1,max} = \mu V_{tot}$$

In Fig. 15b, the friction force at the base, $H_{1,max}$ is too small to prevent the base from sliding backwards. This is generally the case for cohesionless soils. Hence from Figs. 15b and 15c

$$H + H_{1,max} + H_2 > 0 \qquad (3.1)$$

The foundation rotates about a rotation center above the base, so that passive soil pressures develop at the bottom part of the rear vertical face and that H_3 maintains horizontal equilibrium:

$$H + H_{1,max} + H_2 + H_3 = 0$$

For equilibrium, the rotation center cannot be at the base, and should be at some distance above the base. This is generally the case for cohesionless soils where $H_{1,max}$ is rather small (Fig. 15b). The location of the rotation center can be determined from the equations of equilibrium.

The design equations are derived as follows:

If σ_{bc} = the gross bearing capacity of the soil

μ = friction coefficient between sand and concrete

$$H_{1,max} = -\mu V_{tot} \qquad (3.2)$$

$$H_2 = \frac{1}{2} \gamma B Y_{rc}^2 (K_p - K_a) \quad \text{(for cohesionless soils)} \qquad (3.3)$$

$$H_3 = -\{\tfrac{1}{2}\gamma L^2(K_p - K_a) - \tfrac{1}{2}\gamma Y_{rc}^2 (K_p - K_a)\} B \qquad (3.4)$$

$$\Sigma F_y = 0 \text{ gives } X_{rc} = \frac{-2V_{tot}}{\sigma_{bc} B} \qquad (3.5)$$

(the tension part of the pressure diagram at the base is ignored)

$$\Sigma F_x = 0 \text{ gives } H + H_{1,max} + H_2 + H_3 = 0 \qquad (3.6)$$

Substitution of the values of $H_{1,max}$, H_2, and H_3 in Equation 3.6 gives a quadratic equation in Y_{rc}.

The distance Y_3 in Fig. 16 is computed as follows:

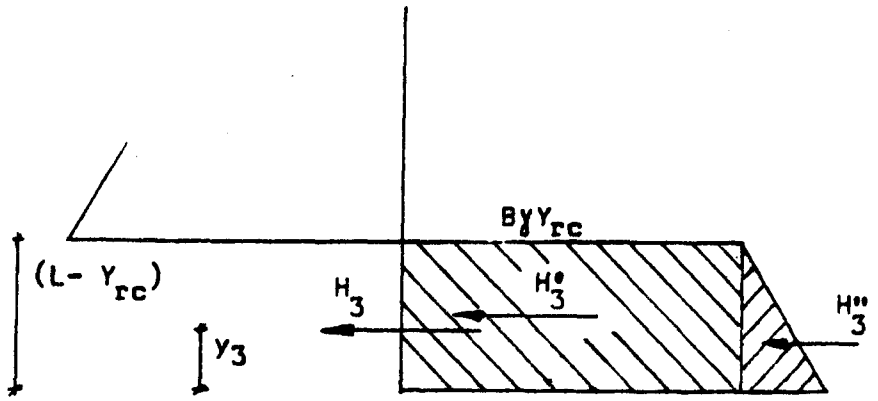

Figure 16. Pressure Diagram for the Lower Part of the Block Foundation

$$H_3 Y_3 = H'_3 \left(\frac{L - Y_{rc}}{2}\right) + H''_3 \left(\frac{L - Y_{rc}}{3}\right)$$

$$Y_3 = \{B\gamma Y_{rc}(L - Y_{rc})(K_p - K_a) \left(\frac{L - Y_{rc}}{2}\right) + \frac{B\gamma(L - Y_{rc})^2 (K_p - K_a)}{2} *$$

$$\left(\frac{L - Y_{rc}}{3}\right) \} / H_3$$

$$Y_3 = \{\frac{B\gamma(K_p - K_a)(L - Y_{rc})^2(2Y_{rc} + L)}{6}\} / -H_3 \qquad (3.7)$$

and the ultimate moment M_{max} is obtained from $\Sigma M_0 = 0$ (Figs. 15b, 15c and 16)

$$M_{max} = \{-HL - H_2(L - \frac{2Y_{rc}}{3}) - H_3Y_3 - (\frac{B}{2}\sigma_{bc}X_{rc})(\frac{D}{2} - \frac{X_{rc}}{3})\} \qquad (3.8)$$

Three equations are available (Equations 3.5, 3.6 and 3.8). Two quantities are "fixed" unknowns: X_{rc} and Y_{rc}. The third unknown is the optional quantity. For given values of M_{max}, H, and V_{tot}, the dimensions B, D, and L are unknowns, but by assuming two of the three values, the third value can be solved with the three equations (the optional quantity). To avoid lengthy calculations, it is best to assume B and L. Equation 3.6 gives Y_{rc} and Equation 3.7 gives Y_3. The value of D is then computed using Equation 3.8.

Note:

1. For cohesive soils, Fig. 15a is used. For

   $H + H_{1max} + H_2 > 0$

   the foundation rotates so that passive soil pressures develop at the bottom part of the rear vertical face and that H_3 maintains horizontal equilibrium,

   $\Sigma H = 0$

   $$H + H_{1max} + H_2 + H_3 = 0 \qquad (3.9)$$

   where $$H_{1max} = (B * D)\ 0.67c + V\tan\frac{2\phi}{3} \qquad (3.10)$$

   where c = cohesion and $\phi' = 0$ ("quick load")

   $$P_p = \gamma y \tan^2(45 + \frac{\phi'}{2}) + 2c' \tan(45 + \frac{\phi'}{2}) = \gamma y + 2c$$

$P_a = \gamma y \tan^2(45 - \frac{\phi'}{2}) - 2c' \tan(45 - \frac{\phi'}{2}) = \gamma y - 2c$

The cohesion c is equal to c' (apparent cohesion)

The cohesion $c = c_u$ (apparent cohesion under undrained condition)

c_u is the average value for different depths

$$P_p - P_a = 4c \tag{3.11}$$

$$X_{rc} = \frac{-2V}{\sigma_{bc} B} \tag{3.12}$$

σ_{bc} is based on the undrained condition ($\phi = 0$).

$$\sigma_{bc} = cN_c\xi_c\xi_{cd} + qN_q\xi_q\xi_{qd} + \tfrac{1}{2}\gamma BN_\gamma\xi_\gamma \tag{3.13}$$

for $\phi = 0$, N_c, N_q and N_γ (= 0) can be obtained from a Prandtl-Reissner and Caquot-Kerisel table (37) and ξ_c, ξ_q from a de Beer-Vesic table (37). The depthfactors ξ_{cd} and ξ_{qd} can be obtained from the formulas proposed by Hansen (37):

$\xi_{cd} = 1 + 0.4\tan^{-1}(D/B)$

$\xi_{qd} = 1 + 2\tan\phi(1 - \sin\phi)^2 \tan^{-1}(D/B)$

M_{max} is obtained from $\Sigma M = 0$

$$M_{max} = -HL + H_2(L - \frac{Y_{rc}}{2}) + H_3(\frac{L - Y_{rc}}{2}) \tag{3.14}$$

2. It was mentioned that for the ultimate moment capacity, the pressure diagram is generally as shown in Fig. 15b for cohesionless soils. However, for a large vertical force or for other appropriate reasons, the rotation center for cohesionless soils could be at the base if the friction force H_1 at the base is large enough to prevent the base from sliding backwards. The pressure diagram at the side

bearing walls for a cohesionless soil will be as shown in Fig. 17, and the design equations will thus be simplified.

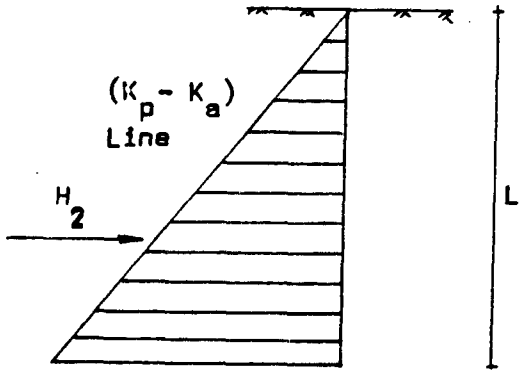

Figure 17. Pressure Diagram at the Ultimate Moment Capacity for Cohesionless Soils (Rotation Center at the Base of the Foundation)

The design procedure, for the rotation center at the base of the foundation, is as follows:

For given M_{max} (acting on the top of the foundation), H, and total vertical load, the dimensions of the block foundation can be obtained by assuming 2 of the 3 values of L, D, and B and solving for the third value. To avoid lengthy calculations, for this particular case B and D are assumed, and L is solved by using Equation 3.11.

3. The equations as derived, are only valid at ultimate soil resistance (ultimate loads).

3.5 Application of the Preliminary Design Equations to the Test Foundation

The equations will be applied to compute the location of the rotation center and the ultimate moment resistance, for given horizontal and vertical forces. The ultimate moment resistance M_u is defined as the maximum "reaction moment" of the soil pressures with respect to the center of the base of the foundation, and the maximum moment M_{max} as the moment acting on top of the foundation as the ultimate moment is reached. The ultimate moment resistance is equal to the sum of the moments (by the ultimate loads) acting on the foundation with respect to the center of the base of the foundation.

As mentioned in Section 2.1.1, for laterally loaded single piles, Broms (5) assumed the maximum lateral passive earth pressures to be three times the passive earth pressures based on Rankine's theory for a cohesionless soil. Downs (10) observed that, for full-scale field tests, the "conventional" Rankine value for laterally loaded single piles was exceeded by a value of five times and more. However, as no explanation has ever been given, an acceptable explanation of the phenomenon is that the three-dimensional arching effect is very influential for a "narrow" pile (Figs. 18b and d), while for a wall with an infinite length the Rankine earth pressure values would be approximated. For passive soil pressures, the Rankine theory assumes that only the soil mass directly in front of the pile is activated for the soil resistance (Fig. 18c). The magnitude of B (Fig. 18c) apparently determines a "correction coefficient" to the Rankine earth pressure values. For a "narrow" wall the soil mass contributing to the soil resistance approximates the area

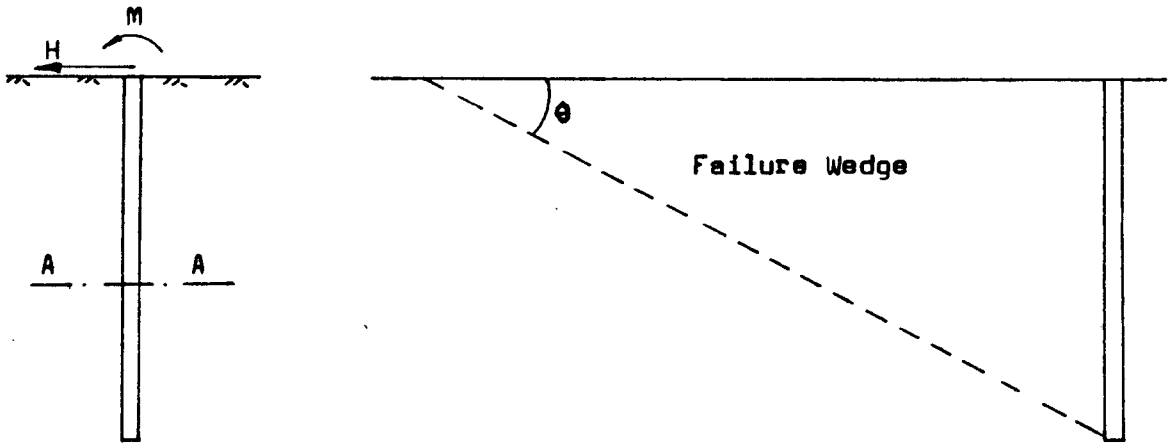

a. Loads

b. Failure Wedge and Failure Plane

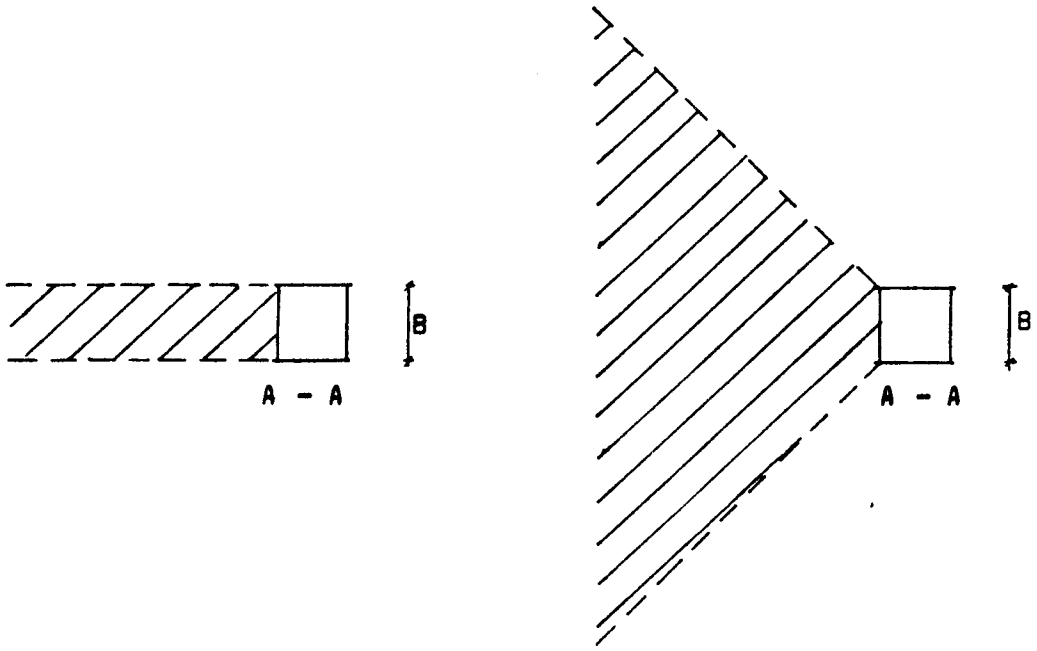

c. Pile Section and Mobilized Soil Mass Contributing to Soil Resistance

d. Pile Section and Mobilized Soil Mass Contributing to Soil Resistance

Figure 18. Failure Wedge and Failure Planes

in Fig. 18d, while for a "long" wall the soil mass contributing to the soil resistance approximates the area in Fig. 18c.

A block foundation is neither "narrow" nor "long." For the test foundation (Fig. 19), the ultimate moment resistance is computed and the maximum soil pressures are assumed to be 1 and 2½ times the lateral pressures based on Rankine's theory. As the results will be needed for later comparisons (Chapter 6), two different load cases will be considered:

Load Case I: V_{tot} = -19,110 lbs (total vertical load)

H = -4,980 lbs (horizontal load)

Load Case II: V_{tot} = -19,110 lbs

H = -10,980 lbs

The rotation centers for the four load cases will also be computed. Data are as follows:

ϕ = 45° (sand); ϕ = 28° (loess)

$\tan^2(45 + \frac{\phi}{2}) = K_p = 5.828$

$\tan^2(45 - \frac{\phi}{2}) = K_a = 0.172$

γ_s = 94.5 lbs/ft^3 (sand backfill)

γ_L = 113 lbs/ft^3 (loess)

γ_c = 150 lbs/ft^3 (concrete)

μ = 0.57 (friction coefficient between sand and concrete)

σ_{bc} = 21,480 psf (Appendix A)

Note: The thin sand layer at the base of the foundation (2 inch) was assumed to have no effect on the bearing capacity (loess). The coefficient of friction however was based on this sand layer.

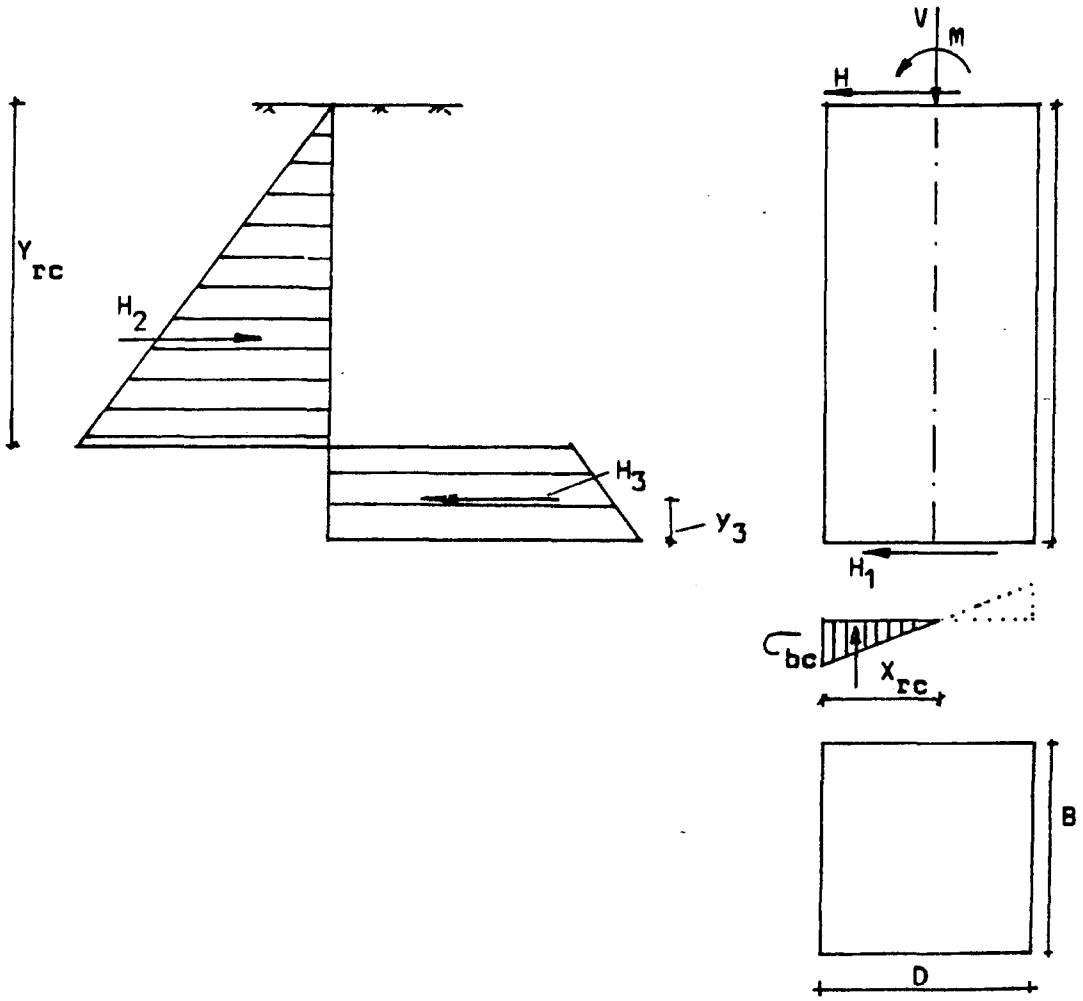

Figure 19. Test Foundation and Pressure Diagrams

B = 3 ft D = 3 ft L = 7 ft

Load Case I: For soil pressures equal to one times the values based on Rankine's theory:

V_{tot} = -19,110 lbs

H = -4,980 lbs

$$X_{rc} = \frac{-2V_{tot}}{\sigma_{bc}B} \tag{3.5}$$

$X_{rc} = 0.593$ ft (Appendix A)

$$H_2 = \tfrac{1}{2}\gamma B Y_{rc}^2 (K_p - K_a) \tag{3.3}$$

$$H_3 = -\tfrac{1}{2}\gamma B(K_p - K_a)(L^2 - Y_{rc}^2) \tag{3.4}$$

$$H_{1,max} = \mu V_{tot}$$

$$H + H_{1,max} + H_2 + H_3 = 0 \tag{3.6}$$

$Y_{rc} = 5.87$ ft

Using Equations 3.3, 3.4, and 3.7 respectively, H_2, H_3, and Y_3 are obtained.

$H_2 = 27{,}579$ lbs $\quad H_3 = -11{,}706$ lbs $\quad Y_3 = 0.546$

Using Equation 3.8:

$$M_{max} = -HL + H_2\left(L - \frac{2Y_{rc}}{3}\right) - H_3Y_3 + \left(\frac{B}{2}\sigma_{bc}X_{rc}\right)\left(\frac{D}{2} - \frac{X_{rc}}{3}\right)$$

$M_{max} = -68{,}762$ lb-ft

$M_{ultimate} = M_{max} + HL = -103{,}600$ lb-ft

These values of M_{max} and Y_{rc} were evaluated for the original Rankine values.

M_{max} and Y_{rc} are now evaluated for soil pressures 2½ times as large as the pressures based on Rankine's theory. The equations based on a "correction factor" of 2½ are:

$$H_{1,max} = -\mu V_{tot} \tag{3.2a}$$

$$H_2 = \frac{5}{4}\gamma B Y_{rc}^2 (K_p - K_a) \tag{3.3a}$$

$$H_3 = -\frac{5}{4}B\gamma L^2(K_p - K_a)(1 - Y_{rc}^2) \qquad (3.4a)$$

$$X_{rc} = \frac{-2V_{tot}}{\sigma_{bc}} \qquad (3.5a)$$

$$H + H_{1,max} + H_2 + H_3 = 0 \qquad (3.6a)$$

$$Y_3 = \frac{5B\gamma(K_p - K_a)(L - Y_{rc})^2(2Y_{rc} + L)}{-12H_3} \qquad (3.7a)$$

$$M_{max} = \{-HL - H_2(L - \frac{2Y_{rc}}{3} - H_3Y_3 - (\frac{B}{2}\sigma_{bc}X_{rc})(\frac{D}{2} - \frac{X_{rc}}{3})\} \qquad (3.8a)$$

using the equations,

X_{rc} = 0.593 ft (Appendix A)

Y_{rc} = 5.335 ft

M_{max} = -153,757 lb-ft

$M_u = M_{max} + H * L$ = -188,600 lb-ft

Load Case II: For the soil pressures equal to the original Rankine values:

V_{tot} = -19,110 lbs

H = -10,980 lbs

X_{rc} = 0.593 ft

Y_{rc} = 6.16 ft

M_{max} = -32,679 lb-ft

$M_{ultimate} = M_u$ = -32,679 + -10,980 * 7 = -109,540 lb-ft

For the soil pressures equal to 2½ times the pressures based on Rankine's theory:

X_{rc} = 0.593 ft

Y_{rc} = 5.466 ft

M_{max} = 121,292 lb-ft

M_u = -198,150 lb-ft ($M_u = M_{max} + H * L$)

The results for Load Cases I and II are presented in tabular form (Table 1).

3.6 Discussion

Rotation center. From the above analysis it can be concluded that the ultimate moment is a function of the rotation center. The location of the rotation center is a function of the total friction force at the base of the foundation and the type of soil and cannot be assumed to be the same for all types of soils as has been previously assumed (6, 28, 31).

Ultimate moment. Table 1 shows the ultimated moments (M_u) computed by using the preliminary design equations for cohesionless soils.

It is seen that the ultimate moment capacity increases with an increase of the horizontal force. This is logical for it can be observed in Fig. 19 that an increase in H causes H_2 to increase ($\Sigma H = 0$), which causes the increase of the resisting moment (this can be seen by taking the moment about the base). Since the rotation point moves toward the base, H_3 decreases, which causes the increase of the ultimate moment capacity. It is also seen that the increase of M_u is rather small (about 5%) for an increase in the horizontal force of more than 100%.

Design for cohesive soils (Figs. 15a and c). For cohesive soils, Equations 3.9 through 3.14 should be used according to Fig. 15a (Section 3.4). It is seen that the design equations for cohesive soils are more simple than those for cohesionless soils.

Table 1. The Maximum Moment, the Ultimate Moment Capacity and the Rotation Center for Soil Pressures Equal to 1 Times and 2½ Times the Values Based on Rankine's Theory

Total Vertical Loads (lb)	Total Horizontal Loads (lb)	Rotation Center X_{rc} for Original Rankine Values (ft)	Rotation Center Y_{rc} for Original Rankine Values (ft)	Rotation Center X_{rc} for 2½ Times Rankine Values (ft)	Rotation Center Y_{rc} for 2½ Times Rankine Values (ft)	Maximum Moment for Original Rankine Values (lb-ft)	Maximum Moment for 2½ Times Rankine Values (lb-ft)	Ultimate Moment Resistance for Original Rankine Values M_u (lb-ft)	Ultimate Moment Resistance for 2½ Times Rankine Values M_u (lb-ft)
19,110	4,980	0.593	5.87	0.593	5.335	68,760	153,760	103,600	188,620
19,110	10,890	0.593	6.175	0.593	5.473	32,680	121,290	109,500	198,150

CHAPTER 4

EXPERIMENTAL PROJECT

4.1 Background

The full-scale test described in the following section has been conducted as an initial phase to provide data on the ultimate resistance of a laterally loaded block foundation. Another objective was to obtain data for lateral soil pressures at specific points of the loaded foundation. Although it was realized that one test would be insufficient to supply meaningful data, it was hoped that enough data would be obtained to be of practical use in the derivation of design equations of side bearing block foundations.

For the design of the foundation we have two decisive limits:

A. An allowable lateral displacement (Appendix F).

B. The ultimate soil resistance needed for the factored loads on which the structural design of the foundation is based.

It was believed that the ultimate moment capacity of the foundation would be indicated by a sudden increase in the "deflection rate" of the foundation. The results obtained from the experimental data will be compared to the results from the derived equations and from the finite-element computer program.

4.2 Equipment and Test Foundation

A reinforced concrete block foundation (3x3x7 ft) was used in the test. The soil in situ was loess. The remaining space of the hole (8x8x7 ft) was backfilled with sand and dry tamped with a 250 lb mechanical tamper. A vertical steel column (W14x61), embedded and fixed

in the foundation, was used for the application of horizontal and vertical loads which caused the overturning moments. To facilitate the application of these loads, a framework was constructed at the top of the column as shown in Fig. 20. The vertical loads were applied by means of a device consisting of a leverarm and load box 1 (Fig. 21a), which caused tension forces in a cable connected by a pulley to the end of the frame, as shown in Fig. 20. Two reinforced concrete auxiliary foundations were needed for this device (Fig. 20). The horizontal components of the forces in the cable to the left and to the right of the frame neutralized each other as the slope of the cable to the auxiliary foundation on each side was 32.25°. The horizontal loads were applied by means of another device consisting of a leverarm and load box 2 (Fig. 21b), which caused tension forces in a cable, sloping upwards with an angle of 29° and connected to the top of the frame (Fig. 20). Another auxiliary foundation was needed for this device (Fig. 20). To measure horizontal soil pressures at arbitrary points in the side bearing walls and soil pressures at the base of the foundation, steel boxes were used, each containing two strain gages (Fig. 24), glued opposite to each other on a steel rod. This steel rod is welded to the pressure face (circular steel plate). The pressures were computed from the readings obtained with the use of a strain gage indicator. A total of 44 boxes and 5 strain gage indicators were used. On each side-bearing wall, 6 rows of boxes were placed, each row consisting of three boxes (Fig. 22). Eight boxes were placed at the bottom (Fig. 23).

The tensions in the cables obtained by the system of the leverarms were checked by placing a strain gage on a transducer in each cable.

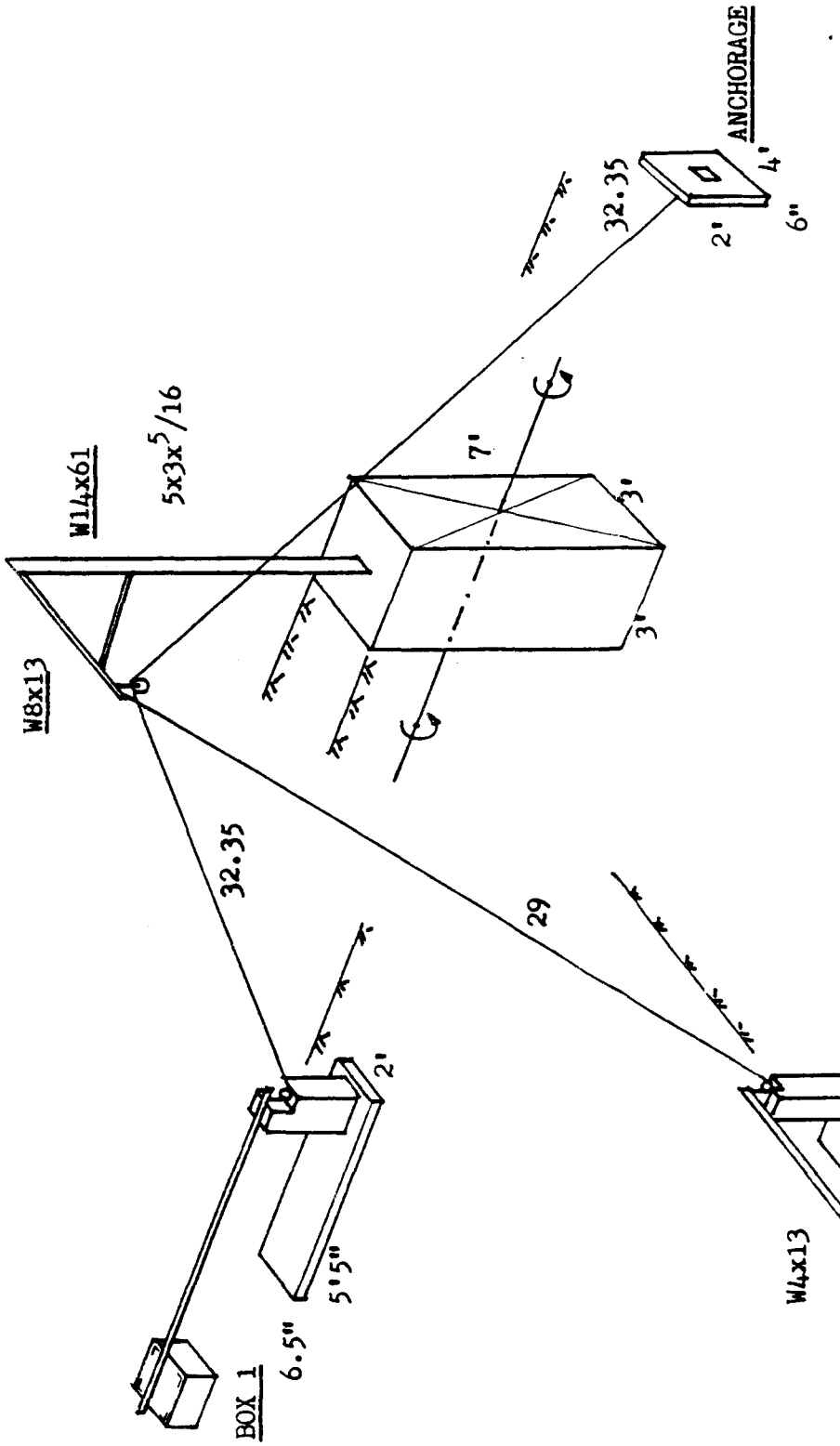

Figure 20 - FOUNDATIONS & LEVERARM SYSTEMS

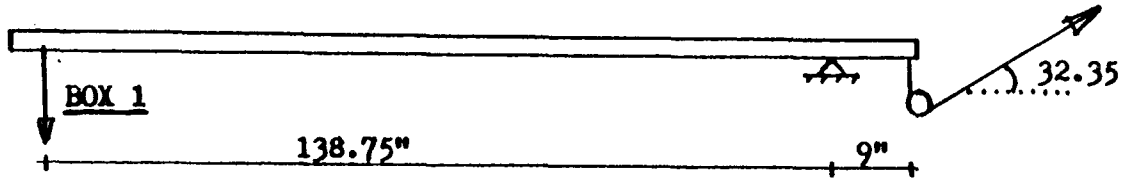

a. LEVERARM SYSTEM & LOAD BOX 1

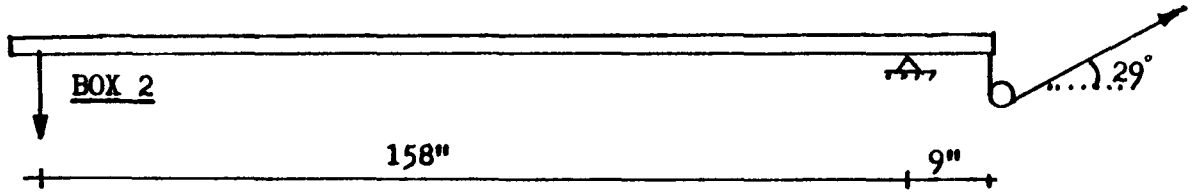

b. LEVERARM SYSTEM & LOAD BOX 2

Figure 21. LEVERARM SYSTEMS

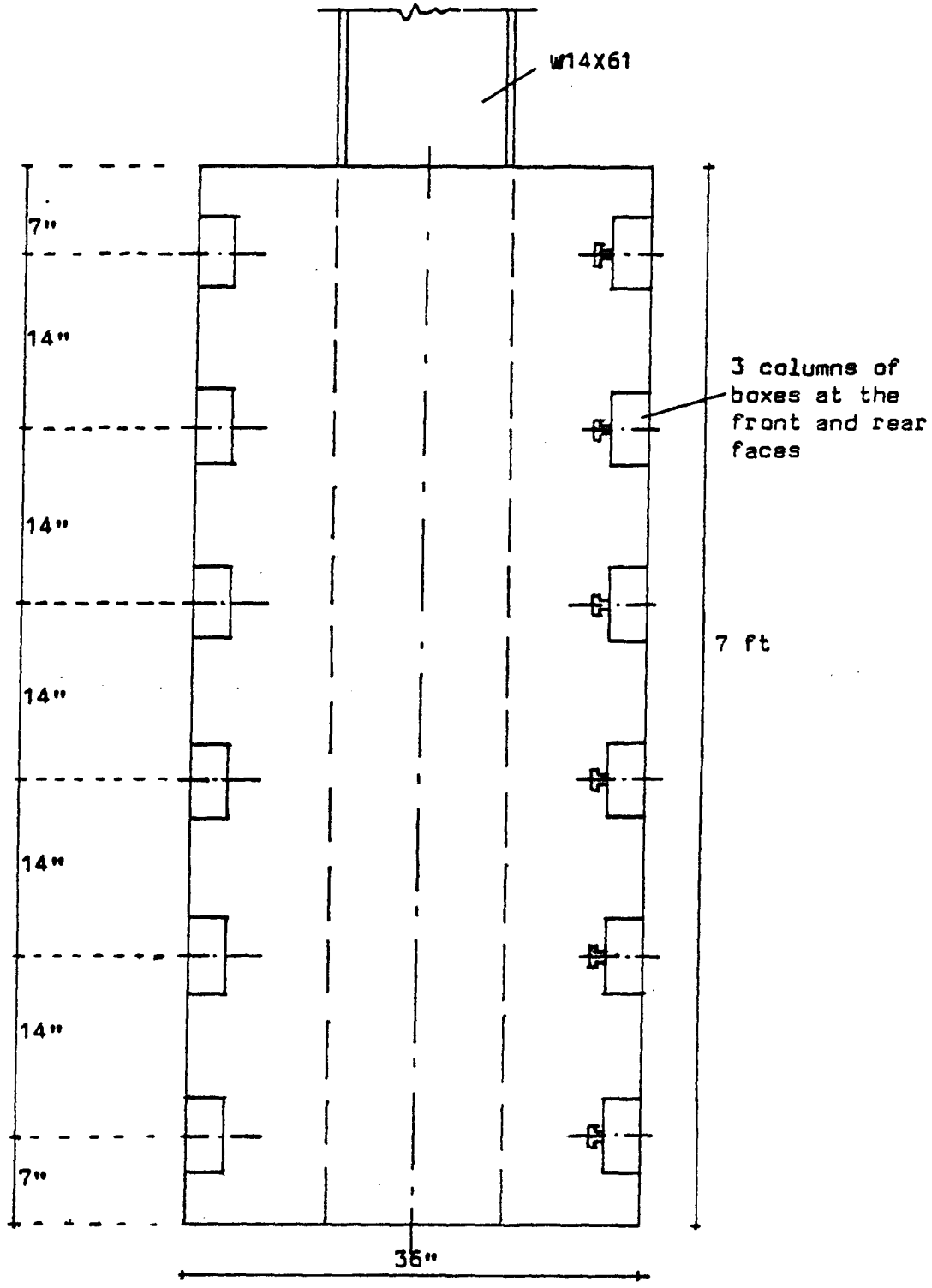

Figure 22. Strain Gage Boxes at the Side Bearing Walls

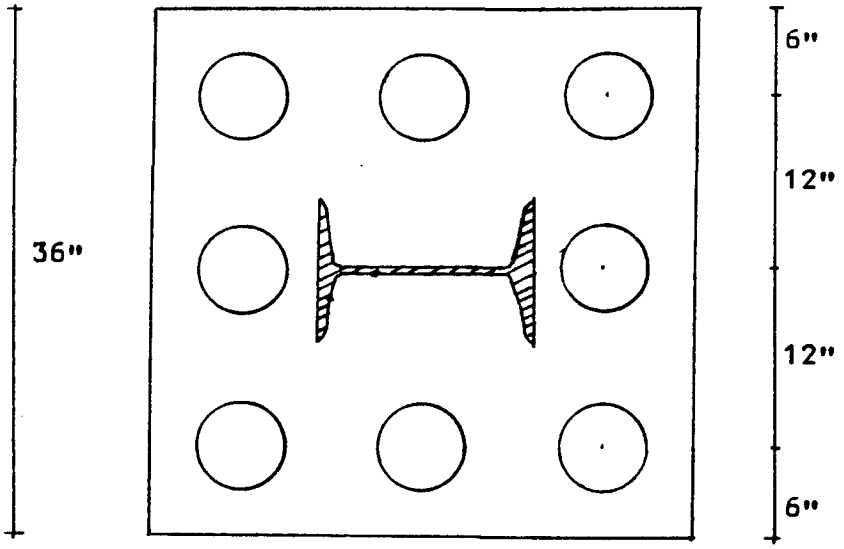

Figure 23. 8 Strain Gage Boxes at the Bottom of the Foundation

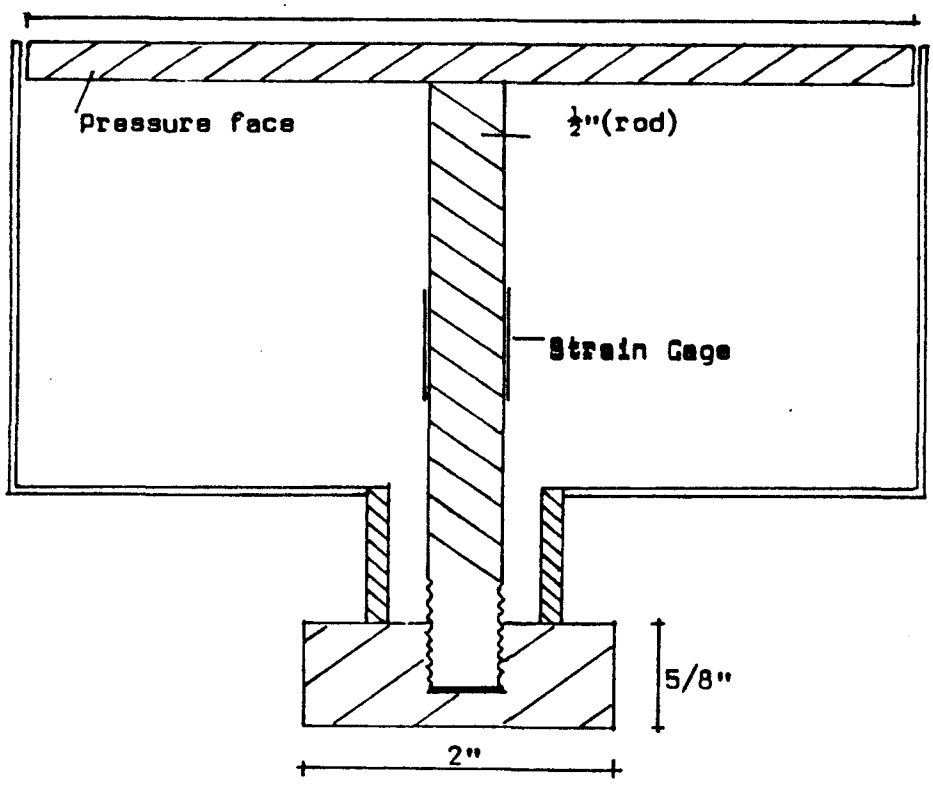

Figure 24. Strain Gage Box

4.3 Test Procedure

The test was performed at the Test Track in Pullman, WA, on September 27, 1984. The soil in situ was loess. A 2-inch tamped sand layer formed the base of the 3x3x7 ft reinforced concrete foundation. Before the concrete was placed, eight boxes complete with the pressure faces, rods and waterproofed strain gages were installed at the bottom of the foundation, the cables being protected by paralon pipes. To place the system of strain gage boxes in the side bearing walls, only the boxes were fastened to the formwork. After the concrete for the foundation was placed, the steel circular pressure faces were screwed to the boxes (after the removal of the formwork). The cables to the surface were protected by paralon pipes, and the remaining space of the hole (8x8x7 ft) was backfilled with sand and tamped with a 250 lbs mechanical tamper until the sand was dense.

The loading sequence and the necessary related activities at the site were as follows:

First step: System of connection of the strain gages to the strain gage indicators.

Second step: Application of vertical loads.

Third step: Application of horizontal loads.

The activities in the field as mentioned above took about nine hours to complete.

First step: System of connection of the strain gages to the strain gage indicators. The two "active" strain gages in the box with two additional "dummy" strain gages were connected in a Wheatstone Bridge (Fig. 25). The objectives of the four arm bridge connection were:

(a) to measure axial strain, (b) to eliminate bending strain, and (c) to achieve temperature compensation.

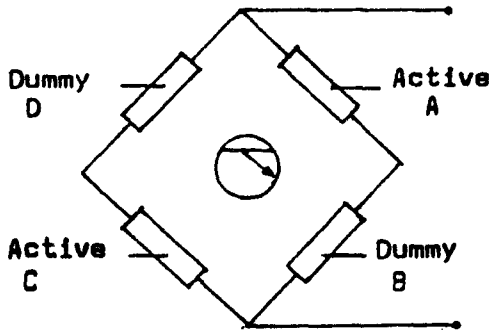

Figure 25. Four Arm Bridge Connection: Applied Circuit

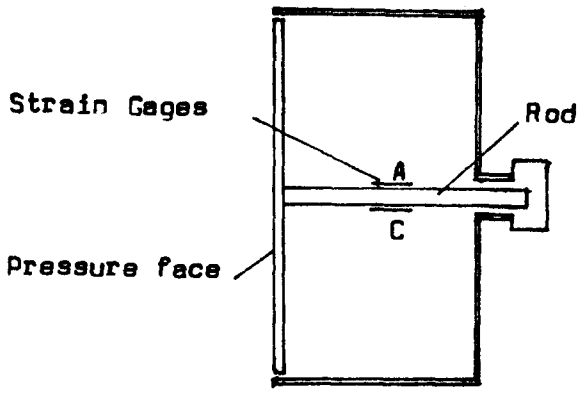

Figure 26. Box with Rod, Pressure Face and Strain Gages

The active gages in the boxes were in the ground, and the dummies which were glued on a steel rod were laid on the ground at about the same location (protected from direct sunlight). The applied circuit was expected to fulfill the three objectives since:

$$\frac{R_A}{R_B} = \frac{R_D}{R_C}$$

Axial strain was measured with double sensitivity since the ratio R_A/R_B decreases while R_D/R_C increases if R_A and R_C decrease (compression). The bending is compensated (Fig. 26) since R_C decreases if R_A increases at the same rate (and vice versa) and the ratio R_A/R_B would still be equal to R_D/R_C.

The applied circuit was also expected to have temperature compensation as the temperature increase at ground level and in the ground was supposed to be the same, so the ratio R_A/R_B for an increase of temperature would still be equal to R_D/R_C. As will be later seen, this last assumption was not true (Appendix C). The dummy strain gages had the same apparent strain characteristics as the active ones, and were mounted on the same material as the active ones.

Second step: Application of vertical loads. Vertical loads were applied in increments at load box 1 resulting in moments and magnified vertical loads acting on the foundation. During this loading, no horizontal forces were acting on the foundation, as the horizontal components of the forces in the cable to the left and to the right of the pulley cancel each other out (the slope to the left and right of the frame were made equal).

At this stage and at most load increments, the horizontal and vertical movements of the top of the foundation were measured by using a transit and a level (Fig. 27).

Readings at the strain gages were recorded at each load increment.

Third step: Application of horizontal loads. While keeping the vertical load on the foundation at about 6,600 lbs, incremental horizontal loads were applied to the foundation. By applying a load at box 2 (Fig. 20), a tension force was created in the cable connected to the framework. This force produced not only a horizontal load, but also a vertical load to the foundation. As it was desired to keep the vertical load constant (at about 6,600 lbs), the load in box 1 had to be decreased as the load in box 2 increased; vertical loads were applied in increments at load box 2, resulting in moments and magnified vertical loads and horizontal loads on the foundation. The load in box 1 was decreased accordingly in order to keep the vertical load to the frame at about 6,600 lbs.

At most load increments, the horizontal and vertical movements of the top of the foundation were recorded using a transit and a level (Fig. 27).

Readings at the strain gages were also recorded.

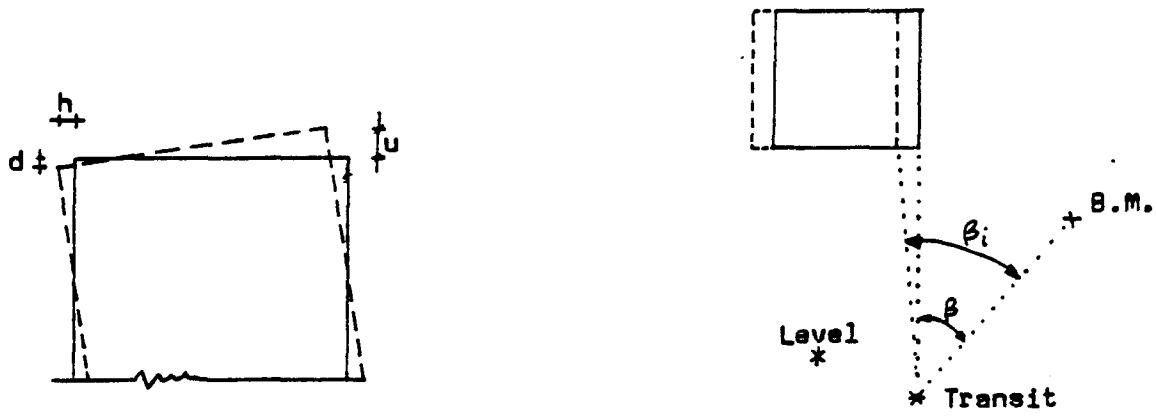

a. Side Elevation b. Top View

Figure 27. Horizontal and Vertical Movements of the Foundation

4.4 Test Results

During the second step, incremental loads were successively applied four times at box 1 (Fig. 20). The magnification ratio of a vertical weight in box 1 to the tension in the cable (Fig. 21a) is: 138.75"/9" = 15.42 lb/lb. A weight of 1 lb at box 1 will induce (Fig. 20) a vertical load at the foundation of 15.42 * 2 sin32.35° = 16.5 lbs. As the distance from the pulley (where the cable is connected) to the center of the foundation is 6.98 ft, the 1-lb weight in box 1 will induce a moment of 16.5 * 6.98 = 115.17 lb-ft at the foundation center. The component horizontal forces cancel each other out. The recorded transit value of β and β_i (Fig. 27) gave the value of $h = R(\beta_i - \beta)$, where R = 15.63' = 4764 mm and β = 51°14' (d and u [Fig. 27] where recorded with the level, where at the "static" load u, d and h were assumed to be 0). The results are as follows:

Table 2. Loads Applied at Foundation from Load Box 1 (Step 2)

Load Increment	Load at Box 1 (lbs)	Vertical Loads at Center of Foundation (lbs)	Moment (lb-ft)	d (mm)	u (mm)	h (mm)
1	71	1,170	8,170	---	---	---
2	171	2,820	19,680	---	---	0.692
3	271	4,470	31,200	0.5	0.5	1.386
4	397	6,550	45,210	---	---	3.464

Note: The values of the moments are the values for the loads acting about the center of the base of the foundation (caused by the loads from load box 1 only).

During the third step, incremental loads were successively applied six times at box 2, while the load at box 1 was decreased accordingly, to keep the "total" vertical load at about 6,600 lbs (for the calculations see Appendix B). The magnification ratio of a vertical load of 1 lb in box 2 to the vertical load induced at the end of the frame (Figs. 20 and 21b) is (158"/9") sin29° = 8.51 lb/lb. The magnification ratio of a vertical load of 1 lb at box 2 to the induced horizontal force acting at the top of the frame (Figs. 20 and 21b) is (158"/9") cos29° = 15.35 lb/lb. As the distance from the top of the frame to the base of the foundation is 14 ft, the magnification ratio of a vertical load of 1 lb to the induced moment at the bottom of the foundation is:

$$8.51 * 6.98 + 15.35 * 14 = 274.3 \text{ lb/lb-ft}$$

A vertical load of 1 lb induces a moment of 274.3 lb-ft at the foundation center. As in Step 2, the values of d and u were obtained with the level and the transit (at the static load u, d and h were assumed to be 0). The results are as shown in Table 3.

Table 3. Applied Loads at Foundation from Load Box 1 and Box 2 (Step 3)

Load Increment	Vertical Loads by Box 1 (lbs)	Vertical Loads by Box 2 (lbs)	Horizontal Loads by Box 2 (lbs)	Moments by Box 1 (lb-ft)	Moments by Box 2 (lb-ft)	Total Vertical Loads (lb)	Total Horizontal Loads (lbs)	Total Moments (lb-ft)	d (mm)	u (mm)	h (mm)
5	6,550	1,110	2,000	45,720	35,660	7,660	2,000	81,470	4.0	3.5	11.086
6	4,470	1,960	3,530	31,210	63,090	6,430	3,530	94,300	4.5	4.0	14.551
7	3,650	2,810	5,070	25,450	90,520	6,460	5,070	116,070	9.0	5.5	24.251
8	2,820	3,660	6,600	19,690	117,950	6,480	6,600	137,630	10.0	12.5	38.802
9	2,000	4,510	8,140	13,940	145,380	6,510	8,140	159,400	13.0	18.0	52.660
10	1,170	5,360	9,670	8,180	172,810	6,530	9,670	180,960	17.0	22.0	60.518

Note: The values of the moments are the values for the loads acting about the center of the base of the foundation (caused by the loads from Box 1 and Box 2 only).

At the beginning of Step 3, after the application of the horizontal load of 2000 lbs to the top of the foundation (and the related vertical load), a crack in the sand on the surface between the soil and the back of the foundation was observed to have formed. Before this first crack appeared, none was observed to have formed, and although no special attention was given to crack formations, no crack was probably formed before this time, as seven persons present near the location of the crack did not perceive the crack formation. As the loads increased, the crack widened. Although the crack widened at each load increment, a total collapse did not occur even at the final load (Table 3).

Determination of the location of the rotation center of the block foundation. From Fig. 28 and the recorded horizontal and vertical movements of the top of the foundation, the values of X_{rc} and Y_{rc} can be computed as follows:

$$X_{rc} = PO = \frac{d}{d + u} * PQ = \frac{d}{d + u} * D \tag{4.4.1}$$

$$\tan\alpha = \frac{d + u}{D} \tag{4.4.2}$$

$$\tan\beta = \frac{u}{h} \tag{4.4.3}$$

$$\alpha r = \frac{h}{\cos\beta} \tag{4.4.4}$$

$$\cos\gamma = \frac{D - X_{rc}}{r} \tag{4.4.5}$$

$$Y_{rc} = r\sin\gamma \tag{4.4.6}$$

Sample calculations are included in Appendix B. The computed values are tabulated in Table 4. The "static" loads and moments (Table 4) are caused by the weight of the frame, leverarms, etc.

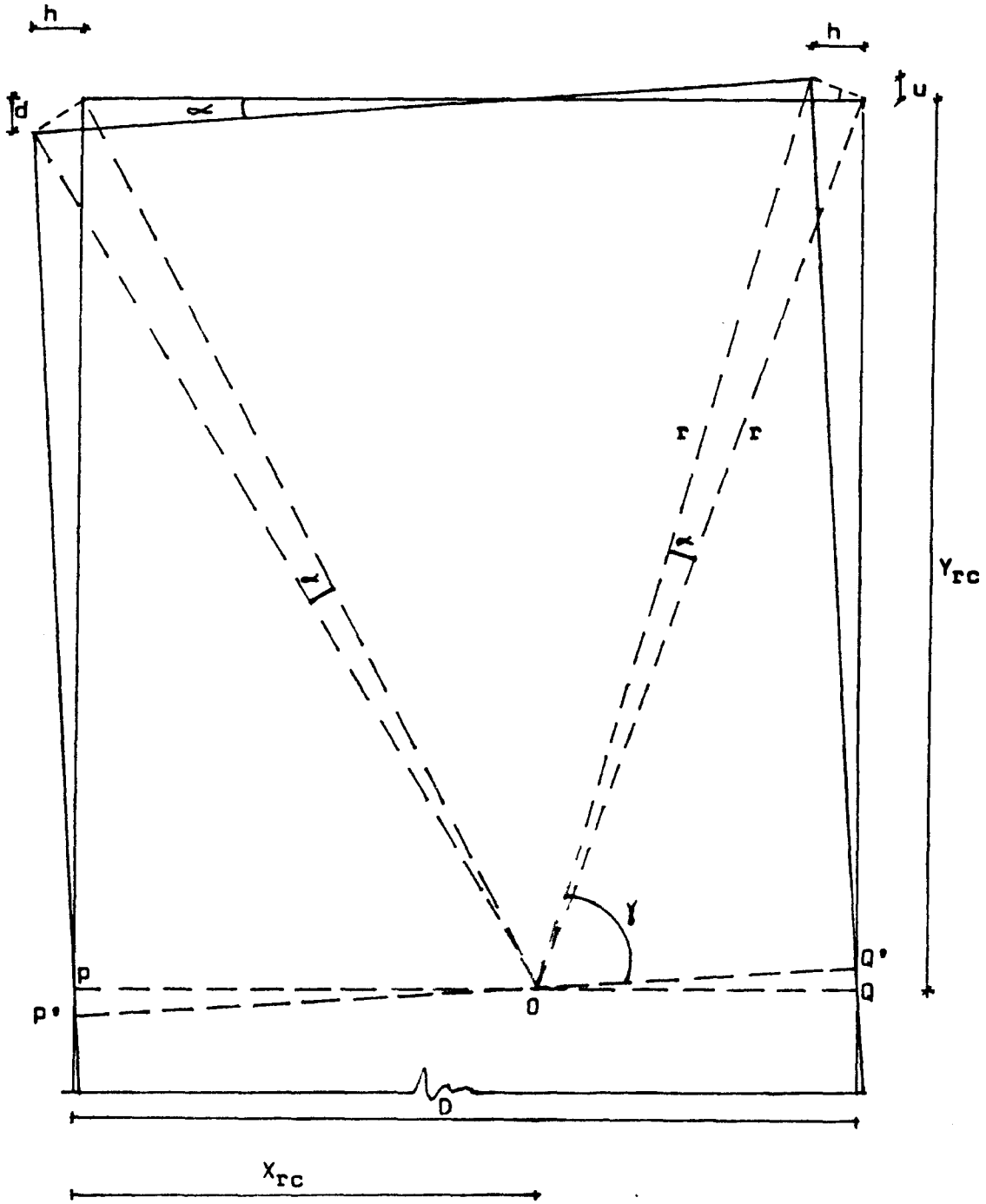

Figure 28. Rotation of the Block Foundation

Table 4. Location of the Rotation Center with Reference to the Applied Loads

Load Increment	Total Horizontal Loads (lbs)	Total Vertical Loads (lbs)	Total Moment Acting on the Center of the Base of the Foundation (lb-ft)	d (mm)	u (mm)	h (mm)	X_{rc} (ft)	Y_{rc} (ft)
1	1,310	13,820	32,210	---	---	---	---	---
2	1,310	15,470	43,180	---	---	0.692	---	---
3	1,310	17,120	54,710	0.5	0.5	1.386	1.50	4.157
4	1,310	19,110	68,710	---	---	3.464	---	---
5	3,310	20,310	104,970	4.0	3.5	11.086	1.600	4.434
6	4,840	19,080	117,800	4.5	4.0	14.551	1.588	5.136
7	6,380	19,110	139,470	9.0	5.5	24.251	1.862	5.02
8	7,910	19,130	161,140	10.0	12.5	38.802	1.333	5.178
9	9,450	19,160	182,820	13.0	18.0	52.660	1.258	5.101
10	10,980	19,180	204,490	17.0	22.0	60.518	1.308	4.652

Note: The total vertical load is equal to the sum of the loading, the weight of the concrete foundation (9,540 lbs) and the "static" vertical load (3,110 lbs). The values of the moments are the values for the loads acting about the center of the base of the foundation. For the total moment, the "static" moment has been included (23,490 lb-ft). For the total horizontal load, the "static" horizontal load (1,310 lbs) has been included.

Horizontal movement of the top of the foundation. The values of the the horizontal movement h of the top of the foundation have been computed from Fig. 27 (at the "static" load, h was assumed to be 0).

$$h = R(\beta_i - \beta_1) \qquad \text{where } R = 15.63' \text{ and } \beta = 51°14'$$

The recorded values of β_i give the subsequent values of h. The tabulated values of h versus the total moment acting about the center of the base of the foundation are presented in tabulated form (Table 5), and are plotted in Fig. 29. The curve in Fig. 29 was obtained by a quadratic least squares approximation. The crack observed between the soil surface and the concrete was measured and is also tabulated in Table 5.

Table 5. Horizontal Movements of the Top of the Foundation

Load Increment	Total Moment Acting About the Center of the Bottom of the Foundation (lb-ft)	Angle	Horizontal Movement of the Top of the Foundation h (mm)	Width of the Crack Between Soil Surface and Concrete (mm)
1	32,210	---	---	---
2	43,180	51°14' 30"	0.692	---
3	54,710	51°15'	1.386	---
4	68,710	51°16' 30"	3.464	---
5	104,970	51°22'	11.086	10.9
6	117,800	51°24' 30"	14.551	15.1
7	139,470	51°31' 30"	24.251	24.8
8	161,140	51°42'	38.802	36.3
9	182,820	51°52'	52.660	50.0
10	204,490	52°02'	60.518	61.0

Strain gage measurements. To measure horizontal soil pressures at arbitrary "points" at the side bearing walls and at the base of the

foundation, strain gage boxes, each containing two strain gages were used (Figs. 22, 23 and 24). To check the computed tension in the cables, obtained by the system of leverarms (Figs. 20 and 21), a device containing one strain gage was placed in each cable. The connection system is described in the first step of Section 4.3. Due to an error in the assumptions of the system, the system did not produce usable results as explained in Appendix C.

4.4.1 Determination of the Ultimate Moment Resistance

Fig. 29 shows that failure is not indicated by a "sudden" increase in the horizontal reflection of the top of the foundation. The load-deflection curve (obtained by a quadratic least squares approximation) showed a peak strength of M_u = 196,200 lb-ft for h = 65.6 mm ($\frac{dM}{dh} = 0$).

The rotation center and horizontal movement of the base of the foundation. It was mentioned in Section 3.4 that generally the maximum friction forces at the base of the foundation are too small to restrain the base from sliding backwards, and that the development of passive soil pressures at the bottom part of the rear vertical face (as the bottom part rotates backwards) ensure the equilibrium of the forces in the X direction. This would mean that the rotation center is above the base of the foundation. The test results show, that for this particular case, the rotation point is above the base.

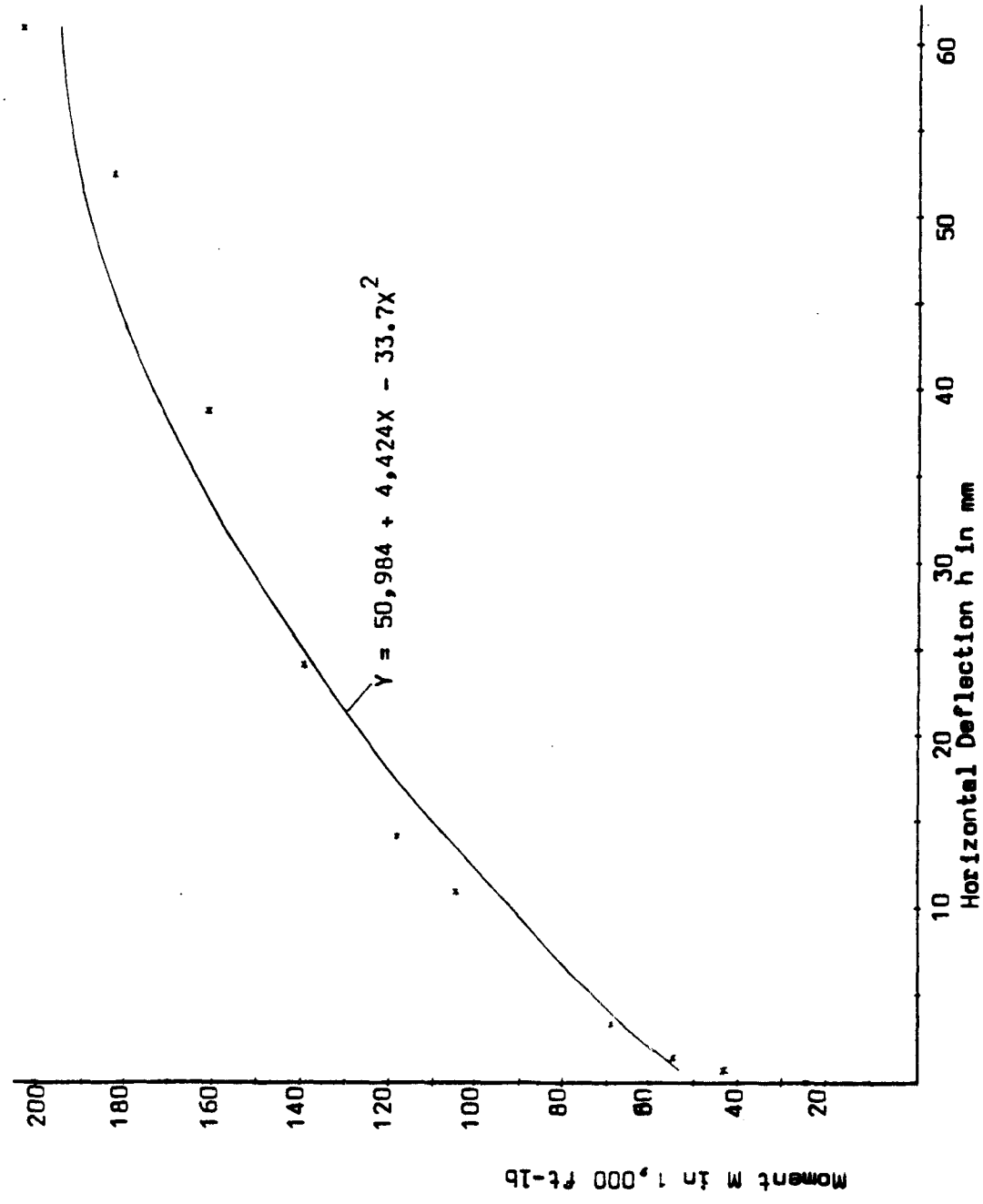

Figure 29. Load - Deflection Curve

CHAPTER 5

COMPUTER PROGRAM

An analysis of the side bearing block foundation was made using a computer program called "ANSYS," an engineering analysis program based on finite elements.

5.1 Discussion of the Model/Results

Finite element mesh. To design the finite element mesh, compromises had to be made so that sufficiently accurate results could be obtained with computer runs of reasonable run time. The smaller the elements the more accurate the results, but the more time is needed to run the program. Several trials had been made before the choice for the mesh was determined. The mesh which was chosen had smaller elements where stress concentration was expected, and larger elements far removed from regions of stress concentration which would not significantly influence the accuracy. The elements which were used were still too large, but the average time to run the program was already up to seven days. The reasons for the time needed was as follows:

- The ANSYS program is resident in the PRIME 400 computer (not sufficiently fast).
- After the yield stress is exceeded, the incremental loads at the successive load steps have to be sufficiently small. If the change in the load is too great, a "fictitious permanent set" is produced which cannot be removed by the corrective iterations of the program (ANSYS: Examples 8.6). In ANSYS, the load increase should not exceed .05P or $(E_T/E)P$, whichever is greater (where E_T = tangent

modulus of the most highly stressed point and E = Young's modulus) (ANSYS: Theoretical Manual 4.1.2). Also, the load increase should not induce a "great" plasticity ratio which is the ratio between the plastic strain increment and the elastic strain. As an example, ANSYS suggests a value for the plasticity ratio of 3 (ANSYS 2.30.5) but no fixed number is set for specific materials.

For the chosen mesh, 115 load steps were needed and for each load step an average of 3 corrective iterations were needed. The load increase was still too great and "permanent set" was produced, but the time to run the program was already too long. For the element aspect ratio (base to height), the findings by Kulhawy (21) were taken into consideration which state that for "soil" problems, a ratio of five in the region of stress concentration, and a ratio of ten away from it, was found to not seriously affect the results. In this solution, the aspect ratio of the soil elements near the concrete foundation was chosen to be two and one-half and, away from the foundation, the aspect ratio was taken as two (Fig. 30).

The mesh boundaries and boundary conditions. The locations of the mesh boundaries and the boundary conditions had to be determined in order to have negligible influence on the problem. After careful consideration, the boundaries and boundary conditions as shown in Fig. 30 were considered to be sufficiently appropriate.

Type and dimensions of the element. For the two-dimensional analysis, two-dimensional isoparametric solid elements with a constant thickness of one inch were used (stif 42). A three-dimensional analysis would require more than the seven days (average) to run the program once.

ANSYS is resident in the PRIME 400 computer (not sufficiently fast for this problem). Stif 12, type 3 (a two dimensional element) was chosen for the interface elements (placed along the boundaries of the soil and concrete) with zero stiffness; interface elements with zero stiffnesses were needed to connect the concrete elements to the cohesionless soil elements which would "otherwise" sustain tension. Stif 12, type 2 was chosen to the other interface elements sustaining compression.

Elastic modulus, stiffness of interface element and Poisson's ratio. The elastic moduli for the soil elements were determined by lab tests (Appendix A); for the cohesionless loess soil, the elastic modulus before the yield stress was reached, was assumed constant at 2,200 psi and for the cohesionless sand soil, was assumed constant at 10,000 psi. As the cohesionless loess and sand are incapable of sustaining tension, the elastic modulus had to be changed to near zero in the direction where tension occurred (average element stress) at the ultimate loads and the problem reanalyzed. After the first run (run until the ultimate load was reached), 61 loess elements and 38 sand elements had to sustain tension in the x or y direction, or in the x and y direction. The elastic modulus for these elements was changed to .001 psi in the direction in which the elements had to sustain tension. This procedure was repeated until at the fifth run only three loess elements and two sand elements showed positive average element stresses, and the results of this run were accepted as the final one.

The Poisson ratios for loess and for sand, were assumed to be 0.25 and 0.35, respectively. Those values were obtained from tables (3) as functions of ϕ.

For the two-dimensional interface elements (stif 12), the analysis is nonconservative. For those interface elements which had to sustain a tensile force the stiffness was set to zero. The stiffnesses of the "noncorner" interface elements are two times the stiffnesses of the corner interface elements.

Yield stresses and bilinear stress-strain curves. For the loess and sand elements, yield stresses were assigned based on the Rankine theory for soil pressures. The nonlinear stress-strain relationship for the soil was simulated by a bilinear curve. The first segment covered the range of stresses up to the yield stress, after which the slope changed to almost horizontal (.001). It was assumed that the yield stresses followed the hydrostatic pattern of the soil pressures based on Rankine's theory, $\gamma y(K_p - K_a)$. Since the yield stress for each element (having a finite height) was constant, the linear distribution of stress could not be maintained. This caused different yield stresses to be assigned to seven adjacent layers. (For the elements near the concrete elements, each layer was subdivided into three sublayers [see Appendix D].)

The gross ultimate bearing capacity of the soil underneath the foundation was 21,480 psf (Appendix A); the ultimate moment resistance was assumed to occur when the yield stress in each of the soil elements adjacent to the interface elements was "exceeded," and the ultimate bearing capacity at the bottom of the foundation was reached.

Friction. The friction coefficient between the base of the concrete foundation and the underlying sand layer has been calculated as 0.57 in accordance with Bowles (2), who recommends $\tan(.667\phi)$ for cohesionless

soils (ϕ = 45° for this case). The friction coefficient between the concrete side bearing wall and the sand was also taken as 0.57.

Considerations of plane strain and plane stress. If the foundation walls were "infinitely" long, as in the case of long stiff retaining walls, there will be only a deformation of the soil elements in the X and Y directions and the condition of plane strain is satisfied. As the walls of the block foundation are not infinitely long, the soil elements will also deform in the Z direction and in this case the condition of plane stress is satisfied. The plain stress assumption for the foundation problem was thought to yield sufficiently accurate results.

Load steps. One hundred-fifteen load steps were needed to obtain the ultimate moment capacity of the foundation. The first load step was chosen so that the stress in one of the elements was slightly greater than the yield stress (ANSYS: Examples 8.6). Subsequent load steps were then needed to arrive at the ultimate loads. The ultimate loads were assumed to have been reached when the yield stresses for all the soil elements adjacent to the interface elements (at the side bearing walls of the foundation) were "exceeded." The increase of the loads in succeeding load steps had to be sufficiently small, as explained previously. An average of three iterations at each load step was needed to achieve "convergence" (the iterative procedure consists of successive corrections to a solution, until equilibrium under the total load is approximated to some acceptable degree). The increase in the loads for succeeding load steps had to be very small, as explained in the discussion for the finite element mesh, and was taken as .05P (ANSYS 2.27.1), and, after the 70th load step, was taken as .006P. The reason for this change in the rate of

the load increase was that, with a load increase of .05P, the increase of the plasticity ratio at the beginning of the load steps was sufficiently small (about .009). However, the rate of increase of the plasticity ratio increased with the increase of the total load, producing a "permanent set." This rate of increase could only be decreased by lowering the rate of load increase.

Others. Ultimate moment resistance and yield stresses. As can be seen from the results of the 115th load step (Appendix E), the yield stresses in the soil were considerably exceeded, although the ANSYS program was supposed to "hold" the soil stresses at the yield stresses (when the yield stresses were exceeded). The reasons for the occurrence were:

A. The rate of load increase was too high, and at each increase when the yield stress was exceeded, the following corrective iterations could not remove the error (ANSYS: Examples 8.6). The rate of the load increase should therefore be decreased; however, more time would be needed to run the program.

B. At the boundary of two elements with different yield stresses, the yield stresses influence each other. Each layer was divided into three sublayers (with the same yield stress). If the layer was subdivided into more sublayers, the "error" would be smaller. But this would mean an increase of the number of elements and an increase of the running time of the program.

With the input used in ANSYS, one run took an average of seven days, and a further change in the present input was found unworkable.

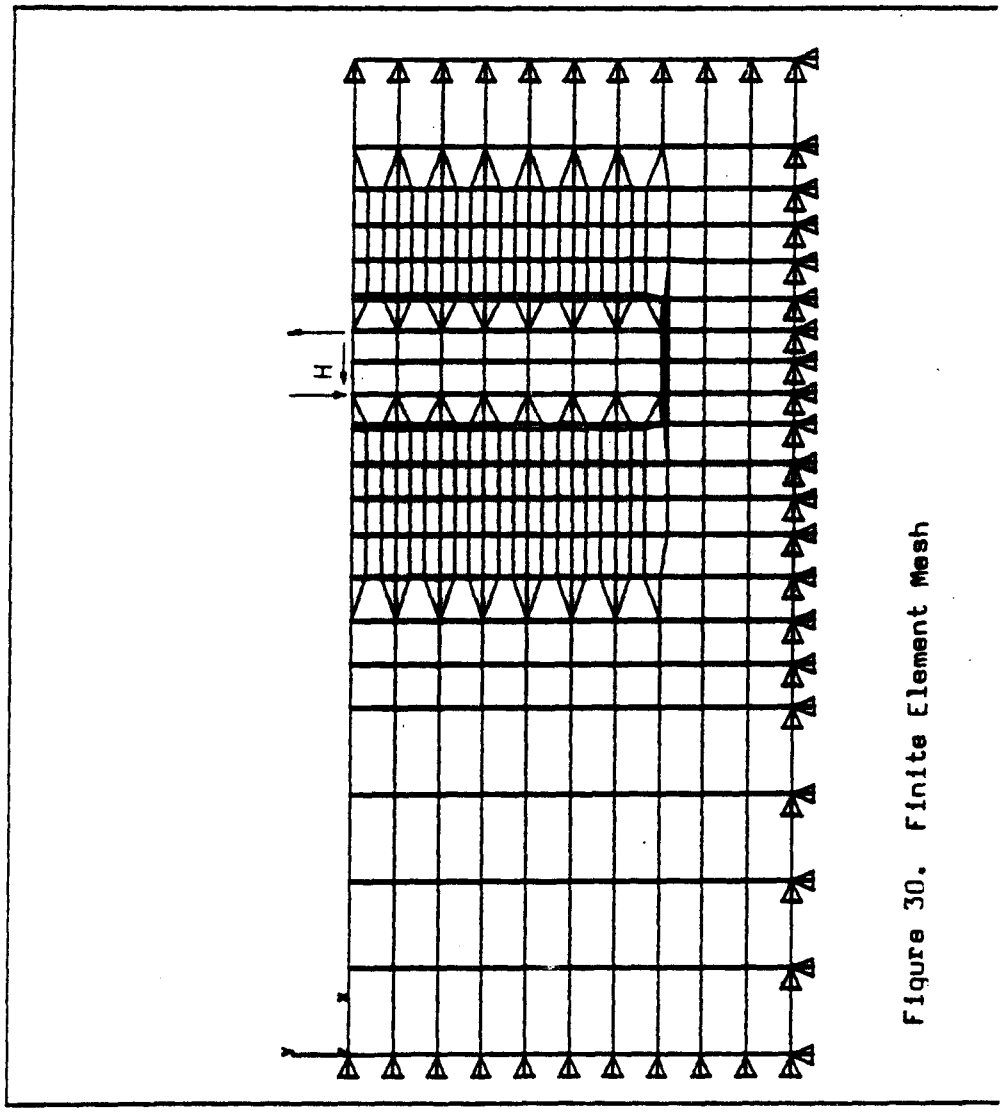

Figure 30. Finite Element Mesh

The ultimate moment resistance was predicted to occur when the yield stresses in all the soil elements adjacent to the interface elements at the side bearing walls were "exceeded," and the bearing capacity at the bottom of the foundation was reached, the latter being 21,480 psf (= 149 psi). At the 115th load step, the soil stresses (for some of the elements near the side bearing walls) were increasing at a rate of about 3 percent. As the soil stresses were already considerably above the yield stresses, this rate of increase, for a succeeding load step, would produce greater inaccuracies in the results. The soil stress at the utmost front of the base was 4,050 psf, not yet near the ultimate bearing capacity. However, for the reason mentioned before, the ultimate moment capacity of the foundation was assumed to have been reached at the 115th load step.

The distance between the forces of the couple acting on the top of the foundation is 18 inches (Fig. 30). At the ultimate moment capacity of the foundation, the "couple forces" acting on the top of the foundation were equal to 1,572 lbs, and the horizontal force H acting on the top of the foundation was equal to 111.9 * 36 = 4,028 lbs. M_{max} = 1,572 * 18 * 36 = 1,018,656 lb-in = 84,900 lb-ft. M_u is needed for practical reasons and found to be M_u = 84,900 + H * 7 = 113,100 lb-ft.

CHAPTER 6

DISCUSSION AND COMPARISONS

For the derivations of practical design equations the following will be compared:

A. The results of the preliminary design equations.

B. The results of the data from the full-scale field test.

C. The results of the finite element approach using the computer program ANSYS.

Table 6. Values of the Ultimate Moment Capacity

	M_u (lb-ft)
Preliminary design equations (Equations 3.2 to 3.8)	109,500
Preliminary design equations (Equations 3.2a to 3.8a)	198,150
Field test	196,200
Finite element/computer program	113,100

The Equations 3.2 to 3.8 were for the original Rankine values while the Equations 3.2a to 3.8a (Section 3.5) were for 2½ times the lateral earth pressures based on Rankine's theory.

The ultimate moments in Table 6 were for the same vertical load V = 19,110 lbs, but for different lateral loads. For the design equations H = -10,980 lbs, for the field test H = -10,980 lbs and for the finite element computer program H = -4,030 lbs. It was found in Section 3.6 that the ultimate moment for H = -10,980 lbs was only 5%

higher than that for H = -4,980 lbs (for a constant V = 19,110 lbs). Therefore, a comparison is possible between the moments in Table 6.

Field test. The field test showed that (for a vertical load of approximately 19,110 lbs and a horizontal load of 10,980 lbs) the ultimate moment resistance is 196,200 lb-ft (Section 4.4). This value was obtained from the curve in Fig. 29. This value is about two times as large as the value for the finite element/computer program and the value for the design equations (for the maximum soil pressures equal to the soil pressures based on Rankine's theory).

Computer program. The results showed M_u to be 113,100 lb-ft, about one-half the ultimate moment obtained from the field test. This was to be expected, as the yield stresses were obtained from the lateral soil stresses based on Rankine's theory and the friction forces at the walls parallel to H were neglected.

Preliminary design equations. In Section 3.3 the ultimate moment resistance for the maximum soil pressures equal to 1 and 2½ times the lateral pressures based on Rankine's theory have been computed. As can be seen, the results for 2½ times the pressures based on Rankine's theory are approximately equal to the results from the load test. This is principally caused by the three-dimensional arching effect (Section 3.5). Another factor contributing to the magnitude of the "correction factor" for the lateral pressures based on Rankine's theory is the friction at the walls parallel to H. For piles (Section 3.5) Broms (5) assumed a correction factor of three and Downs (10) observed that a correction factor of five or more was needed.

In Section 3.5 the "arching effect" was discussed. It was expected that an infinitely long wall would not be affected by the "arching effect" and that the arching effect would be influential for a "narrow" wall.

However, the area of the walls parallel to H determines also the magnitude of the resisting moment and the magnitude of the correction factor.

Therefore, the design equations 3.2a to 3.8a (Section 3.5), based on lateral pressures equal to $2\frac{1}{2}$ times the pressures according to Rankine's theory are only valid for prismatic block foundations having a square base and a ratio of $\frac{L}{D} = \frac{7}{3}$.

CHAPTER 7

CONCLUSION AND RECOMMENDATIONS

7.1 Conclusions

7.1.1 Reliability of the Design Equations

For a prismatic block foundation with a square base: B = D = 3 ft and L = 7 ft, it was observed that the lateral earth pressures based on Rankine's theory had to be multiplied by a "correction factor" of 2½ to obtain an ultimate moment approximately equal to that obtained from the field test. This factor is incorporated in Equations 3.2a to 3.8a (Section 3.5). This correction factor is only valid for a block foundation with the above-mentioned dimensions. This has been discussed in Chapter 6. For better accuracy, the ultimate moment has to be confirmed by more tests at the same site for block foundations with the same dimensions to obtain a more exact coefficient for the lateral earth pressures. For other dimensions or other types of soil or other densities the correction factor would be different.

7.1.2 Rotation Center

From the results at Section 3.5 it is seen that Y_{rc} and M_u increase if the lateral force increases (Sections 3.5 and 3.6). The increase in M_u is relatively small. The values of the rotation center are tabulated in Table 7 (for loading conditions as in Section 6). As can be seen, the rotation center is above the base. Y_{rc} obtained by the three methods compared well to each other.

Table 7. Comparison of the Location of the Rotation Center

	Y_{rc} (ft)	X_{rc} (ft)
Design equations (Equations 3.2a to 3.8a)	5.47	0.59
Field test	5.0	1.3
Finite elements/computer program	4.89	0.32

For the design of side bearing block foundations the existing literature showed that assumptions were made about the location of the rotation center:

a. Simpson and Edwards (31) discussed two methods used in Great Britain (Section 2.1.3). In the first method the rotation center was assumed to be at a depth $\frac{2}{3}L$; in the second method the rotation center was assumed to be at a depth $Z + (\frac{L - Z}{2})$, where Z is the amount of top soil to be neglected.

b. Caquot-Kerisel (6) discussed a French method used in Germany. The rotation center was assumed to be at the base.

c. Seelye (28) assumed the rotation center to be at a depth $\frac{2L}{3}$.

The results from the design equations, field test and finite element/computer program are Y_{rc} = 0.78L, 0.71L and 0.7L, respectively. For a "large" vertical load however, the rotation center should be at the base (Section 3.4).

7.2 Recommendations

The results and conclusions of the present study have led to the following suggestions for further studies in this area.

7.2.1 Field Tests

a. The correction factor of $2\frac{1}{2}$ for the lateral earth pressures based on Rankine's theory (for a prismatic block foundation with a square base: B = D = 3 ft and L = 7 ft) has to be confirmed by more tests. For the same dimensions, tests are required for the same physical conditions (density of backfill, etc.).

   Tests are also needed to determine the influence of the density of the backfill and the influence of the soil in situ (surrounding the backfill) on the correction factor.

b. The correction factors have to be determined for foundations with different B, different $\frac{B}{D}$ and different $\frac{L}{D}$ ratios, since the three-dimensional arching effect and the friction at the walls parallel to H affect the magnitude of the correction factor (Section 6).

7.2.2 Computer Program/Finite Element Formulation

The input to the program was based on a bilinear stress-strain curve (Section 5.1), a simulation of the nonlinear stress-strain curve of the soil. A two-dimensional (stif 42) plane stress element with unit thickness was used. The frictional forces at the walls parallel to the applied forces were neglected, since the analysis was two dimensional.

For more accurate results the following is recommended:

A) A three-dimensional analysis, taking into account the frictional forces at the walls parallel to the horizontal action forces.

B) The load increase should be taken smaller, as has been pointed out in the discussion for the finite element mesh (Section 5.1).

C) An analysis should be made with a more sophisticated stress-strain relationship for the soil.

REFERENCES

1. American Wood Preservers Institute, How to Design Pole-Type Buildings, 3rd Ed., 1962.

2. Bowles, J. E., Analytical and Computer Methods in Foundation Engineering, McGraw-Hill, 1974.

3. Bowles, J. E., Foundation Analysis and Design, McGraw-Hill, 1977.

4. Broms, B. B., "Design of Laterally Loaded Piles," Soil Mechanics and Foundation Division, ASCE, Vol. 92, No. SM3, Proceedings Paper 4342, May 1965, p. 79.

5. Broms, B. B., "Lateral Resistance in Cohesionless Soils," Soil Mechanics and Foundation Division, ASCE, Vol. 90, No. SM3, Proceedings Paper 3909, May 1964, p. 123.

6. Caquot-Kerisel, Grundlagen der Bodenmechanik, Springer Verlag, 1967, S. 376-383.

7. Clough, G. W. and Duncan, J. M., "Finite Element Analysis of Retaining Wall Behavior," Soil Mechanics and Foundation Division, ASCE, Vol. 97, No. SM12, Paper 8583, December 1971.

8. Czerniak, E., Resistance to Overturning of Single Short Piles, ASCE Vol. 83, Proceedings Paper 1188, March 1957.

9. Davisson, M. T. and Prakash, S., "A Review of Soil-Pole Behavior," Highway Research Record, No. 39, 1964.

10. Downs, D. I. and Chieurzzi, R., "Transmission Tower Foundations," Journal of the Power Division, ASCE, Vol. 92, No. PO2, Proc. Paper 4750, April 1966.

11. Desay, Ch. S. and Christian, J. T., Numerical Methods in Geotechnical Engineering, McGraw-Hill, 1977.

12. Drucker, M. A., "Embedment of Poles, Sheeting and Piling," Civil Engineering, No. 12, December 1934.

13. Duncan, J. M., Byrne, P., Wong, K. S. and Mary, P., Strength, Stress-Strain and Bulk Modulus Parameters for Finite Element Analysis in Soil Masses, Report No. UCB/GT/80-01, University of California-Berkeley, August 1980.

14. Engineering Experiment Station, Bulletin No. 3, North Carolina State College, August 1929.

15. Engineering Department Report No. 169, Southern California, Edison Company, March 1963.

16. Fellenius, B. H., "Pile Foundations-Analytical," Section 10 in Analysis and Design of Building Foundations, Fang, H. Y. (ed.), Envo Publishing Company, Inc., 1976.

17. Girijavailabhan, C. V. and Reese, L. V., "Finite-Element Method for Problems in Soil Mechanics," Journal of the Soil Mechanics and Foundation Division, ASCI, Proceedings, Vol. 94, No. ST2, March 1968, pp. 473-496.

18. Gurfinkel, G., Wood Engineering, Upton Printing Company, 1973.

19. Hetenyi, M., Beams on Elastic Foundations, University of Michigan Press, Ann Arbor, 1949.

20. Huntington, W. C., Earth Pressure and Retaining Walls, John Wiley and Sons, Inc., 1957.

21. Kulhawy, F. H., "Embankments and Excavations," Section 16 in Numerical Methods in Geotechnical Engineering, Desai, C. S. and Christian, J. T. (eds.), McGraw-Hill Book Company, 1977.

22. Palmer, L. A. and J. B. Thompson, The Earth Pressure and Deflection along the Embedded Length of Piles Subjected to Lateral Thrust, Proceedings of the 2nd International Conference of Soil Mechanics and Foundation Engineering, Vol. V, P. 156, 1948.

23. Patterson, D., "Pole Building Design," American Wood Preservation Institute, No. 6, October 1968.

24. Poulos, H. C., "Analysis of Piles and Lateral Movements," Soil Mechanics and Foundation Division, ASCE, Vol. 99, 1973, pp. 391-406.

25. Prakash, S., Behavior of Pile Groups Subjected to Lateral Loads," Thesis, University of Illinois, Urbana, 1962.

26. Sandeman, J. W., "Experiments on the Resistance to Horizontal Stress of Timber Piling," Van Nostrand's Engineering Magazine, Vol. XII, New York, 1880, pp. 493-497.

27. Scott, C. R., Soil Mechanics and Foundations, Applied Science LTD, London, 1980.

28. Seelye, E. E., Foundations, John Wiley and Sons, Inc., 1956, pp. 4-16.

29. Selvadurai, A. P. S., Elastic Analysis of Soil-Foundation Interaction, Elsevier Scientific Publishing Company, 1979.

30. Shilts, W. L., Graves, L. D. and Driscol, G. G., A Report of Field and Laboratory Tests on the Stability of Posts Against Lateral Loads, Proceedings of the 2nd International Conference on Soil Mechanics and Foundation Engineering, Vol. V, 1948, pp. 107-122.

31. Simpson, N. G. and Edwards, B. C., "Overhead Transmission Lines," in Civil Engineering Reference Book, Comrie, J. (ed.), Butterworths, London, 1961.

32. Sowers, G. B. and Sowers, G. F., Introductory Soil Mechanics and Foundations, 2nd Ed., The MacMillan Company, New York, 1961.

33. Terzaghi, K., "Large Retaining Wall Tests, I: Pressure of Dry Sand," Engin. News-Rec., Vol. 3, February 1934.

34. Terzaghi, K., "Evaluation of Coefficients of Subgrade Reaction," Geotechnique, Vol. 5, England, 1955.

35. Thornburn, T. H., Peck, R. B. and Hanson, W. E., Foundation Engineering, 2nd Ed., John Wiley and Sons, Inc., 1974.

36. Williams, C. C., The Design of Masonry Structures and Foundations, 2nd Ed., 1930, p. 479.

37. Winterkorn, H. F. and Fang, H. Y., Foundation Engineering Handbook, Van Nostrand & Reinhold Co., 1975.

38. Zeevaert, L., Foundation Engineering, 2nd Ed., Van Nostrand Reinhold Company, 1972.

APPENDIX A

SOIL LAB TESTS AND APPLICATION OF THE DESIGN EQUATIONS

The following soil tests were performed

a. Sand cone test - to determine the density

b. Direct shear test - to determine the angle of internal friction

c. Compressibility test - to determine the elastic modulus

The following were obtained:

For the backfill (sand):

$Q_s = 45°$

$\gamma_s = 94.5$ lbs/ft^3

$E_s = 10{,}000$ psi

$\nu_s = 0.35$ (tabulated)

For the soil in situ (loess):

$Q_L = 28°$

$\gamma_L = 113$ lbs/ft^3

$E_L = 2{,}200$ psi

$\nu_L = 0.25$

The ultimate gross bearing capacity was determined by using 3.13 (Section 3.4).

$$\sigma_{bc} = cN_c\xi_c\xi_{cd} + qN_q\xi_q\xi_{qd} + \tfrac{1}{2}B\gamma N_\gamma\xi_\gamma\xi_{\gamma d}$$

$c = 0$; for $\phi = 28°$:

$N_q = 14.72$ and $N_\gamma = 16.72$ (37)

from a table (37):

$\xi_q = 1.531$; $\xi_\gamma = 0.6$

and the depthfactors:

$$\xi_{qd} = 1 + 2\tan\phi(1 - 2\sin\phi)^2 \tan^{-1}\frac{D}{B} = 1.349$$

$$\xi_{\gamma d} = 1$$

$$\sigma_{bc} = (7 * 94.5)\ 14.72 * 1.531 * 1.34g + \frac{3}{2} * 94.5 * 16.72 * 0.6$$

$$\sigma_{bc} = 21{,}480 \text{ psf}$$

In Section 3.5 the equations were applied to the test foundation. As had been discussed in Section 3.5, three equations (Eqs. 3.5, 3.6 and 3.8) are available with two "fixed" unknowns, X_{rc} and Y_{rc}. The third "optional" unknown in this case is M_{max}, as L, D, and B are known quantities. For the data in Section 3.5, X_{rc}, Y_{rc} and M_{max} are computed as follows:

Sample calculations for Load Case I (see Section 3.5):

(Equation 3.5): $X_{rc} = \frac{2V_{tot}}{\sigma_{bc}B} = \frac{2 * 19{,}110}{21{,}480 * 3} = 0.593$ ft

(Equation 3.3): $H_2 = \frac{1}{2}\gamma B Y_{rc}^2 (K_p - K_a) = \frac{94.5}{2}(3 * 5.656 Y_{rc}^2) = 801.74 Y_{rc}^2$

(Equation 3.4): $H_3 = -\frac{1}{2}\gamma B(K_p - K_a)(L^2 - Y_{rc}^2) = -39{,}285 + 801.74 Y_{rc}^2$

(Equation 3.2): $H_{1,max} = -\mu V_{tot} = -0.57 * 19{,}110 = -10{,}893$ lbs

(Equation 3.6): $H + H_{1,max} + H_2 + H_3 = 0$

$$-4{,}980 - 10{,}893 + 801.74 Y_{rc}^2 - 39{,}285 + 801.74 Y_{rc}^2 = 0$$

$$Y_{rc} = 5.87'$$

Equations 3.3, 3.4 and 3.7 give:

$H_2 = 27{,}579$ lbs $H_3 = -11{,}706$ lbs $Y_3 = 0.546$ ft

Substituting X_{rc}, Y_{rc}, H_2, H_3 and Y_3 into Equation 3.8 gives:

$$M_{max} = -HL + H_2(L - \frac{2Y_{rc}}{3}) - H_3Y_3 + (\frac{3}{2} f_{bc} X_{rc})(\frac{D}{2} - \frac{X_{rc}}{3})$$

$$M_{max} = -68,762 \text{ lb-ft}$$

$$M_u = M_{max} + H * L$$

$$M_u = M_{max} = -103,600 \text{ lb-ft}$$

The results for Load Case I and Load Case II are presented in tabular form (Table 1).

APPENDIX B

CALCULATIONS OF THE MOMENTS AND LOADS ABOUT THE BASE OF THE FOUNDATION AND OF THE LOCATION OF THE ROTATION CENTER

Sample calculations for Step 2: Application of a load at box 1 and the resulting loads to the foundation.

As had been explained in Section 4.4, a vertical weight of 1 lb produces a vertical load of 16.5 lbs at the center of the foundation and an additional moment of 115.7 lb-ft (the magnification ratio of the vertical load is 16.5 and for the moment = 115.17).

For load increment 1, the load of 71 lbs in box 1 induces a vertical load and moment at the foundation equal to:

$$V_{b1} = 16.5 * 71 = 1{,}170 \text{ lbs}$$

$$M_{b1} = 115.17 * 71 = 8{,}170 \text{ lb-ft}$$

Table 2 gives the values of load increment 1 through load increment 4 of Step 2.

Sample calculations for Step 3: Application of a load at box 2 and box 1 and the resulting loads to the foundation.

For box 2, the magnification ratios for the vertical load, the horizontal load, and the moment are: 8.51 lb/lb, 15.35 lb/lb and 274.3 lb/lb-ft, respectively. For load increment 5 with vertical loads of 397 lbs in box 1 and 130 lbs in box 2, the resulting loads are as follows:

For box 1:

$$V_{b1} = 397 * 16.5 = 6{,}550 \text{ lbs}$$

$$M_{b1} = 397 * 115.17 = 45{,}720 \text{ lb-ft}$$

For box 2:

V_{b2} = 130 * 8.51 = 1,110 lbs

H_{b2} = 130 * 15.35 = 2,000 lbs

M_{b2} = 130 * 274.3 = 35,660 (acting at the base of the foundation)

and the total values for box 1 and box 2 at load increment 5:

V_{tot} = 6,550 + 1,110 = 7,660 lbs

H_{tot} = 2,000 lbs

M_{tot} = 45,720 + 35,660 = 81,380 lb-ft

Table 3 gives the values for V, H, and M for load increment 5 through load increment 10.

Sample calculations for the location of the rotation center:

For load increment 5, from the recorded data (Table 4) (see also Fig. 28):

d = 4.0 mm u = 3.5 mm h = 11.086 mm D = 36" R = 15.63 ft

$$X_{rc} = \frac{d}{d + u} D \qquad \text{(Equation 4.4.1)}$$

$$X_{rc} = \frac{4}{7.5} 3 = 1.6 \text{ ft}$$

$$\tan\alpha = \frac{d}{d + u} \qquad \text{(Equation 4.4.2)}$$

$$\tan\alpha = \frac{7.5}{(3 * 12)2.54 * 10} \quad : \quad \alpha = 0.001094 \text{ rad}$$

$$\tan\beta = \frac{u}{h} \qquad \text{(Equation 4.4.3)}$$

$$\tan\beta = \frac{3.5}{11.086} \quad : \quad = 19.8369°$$

$$r = \frac{h}{\alpha\cos\beta} \qquad \text{(Equation 4.4.4)}$$

$$r = \frac{h}{\alpha\cos\beta} = \frac{11.086}{0.001094\cos 19.8369}$$

r = 1417.3 mm = 4.65 ft

$$\cos\gamma = \frac{D - X_{rc}}{r} \qquad \text{(Equation 4.4.5)}$$

$$\cos\gamma = \frac{1.4}{4.65} \quad : \quad \gamma = 72.478$$

$$Y_{rc} = r\sin\gamma \qquad \text{(Equation 4.4.6)}$$

$$Y_{rc} = 4.65 * 0.9536 = 4.434 \text{ ft}$$

The results are tabulated in Table 4.

APPENDIX C

STRAIN MEASUREMENTS AND COMPUTATIONS OF SOIL PRESSURES

The following is a discussion of the approach used in the strain gage indicator recordings and the resulting errors in the computation of the soil stresses.

As had been mentioned in Section 4.3, the objectives of the system of connection of the Wheatstone-bridge circuit (Fig. 25) were:

a) to measure axial strain,

b) to eliminate bending strain, and

c) to achieve temperature compensation.

As explained in Section 4.3, objective b was achieved. However, temperature compensation was not accomplished. For a balanced bridge (Fig. 25),

$$\frac{R_A}{R_B} = \frac{R_D}{R_C}$$

R_A and R_C, the active strain gages, were represented by the two strain gages (Fig. 24) in the strain gage box (placed below the soil surface, "between" the concrete and the soil). R_B and R_D, the "dummies," were laid on the surface of the ground at the same location as the active gages and protected by a jacket from direct sunlight. R_B and R_D were glued on a round rod of the same diameter and material as the rod used with the active strain gages. During the loading process, the temperature increased as the sun shone and a cold wind blew intermittently (with a moderate velocity). As R_A and R_C were glued on the same rod and R_B and R_D on another rod, the temperature increase of R_D was equal to that of R_B, while the temperature increase of R_A was equal

to that of R_C. The increase of the temperature of the rod of R_A and R_C was supposed to be equal to the increase of the temperature of the rod of R_B and R_D.

If this were true, R_A/R_B would be equal R_D/R_C, and temperature compensation would have been achieved. However, as the rod of the latter pair was on the ground while the rod of the former pair was in the ground, the increase of temperature of the latter rod was much less than the former rod. Moreover, as the wind (rather cold) was blowing intermittently over the cover of the dummy gages, the dummy gages were subjected to changing temperatures. The influence of the wind was noticeable, since a drift in the readings was perceived. The readings sometimes changed erratically, even at a static load. An electric line along the road (distance = 35 yards) was at first thought to have been the reason.

An examination of the results after conversion to soil stress values showed that the results were not usable. A few sample readings and computed soil stresses (at the load where the crack between concrete and soil was perceived, i.e., load increment 5 [see Table 3]), will be shown and discussed (see also Fig. 32):

rod diameter = ½"

cross section area of the rod = 0.19635 in^2

diameter of the pressure face = 5-3/4 inch

area of the pressure face = 25.97 in^2

elastic modulus of steel rod = 29 * 10^6 psi

The soil at the initial readings were already in a state of stress. If we take the coefficient of earth pressure at rest for dense sand

$K_0 = 0.4$, and $\gamma_s = 119$ lbs/ft^3, the value of the initial soil stresses at the walls are:

$$\gamma_s Z_i K_0$$

and at the base of the foundation:

$$Z\gamma_{concrete} \text{ (where } \gamma_{concrete} = 150 \text{ lbs/ft}^3)$$

For boxes 8, 6, 7, 22 and 10 (see Table 7 for readings):

$$P_8 = 29 * 10^6 * \left(\frac{4,580 - 4,482}{2}\right) * 10^{-6} * 0.19635 = 279 \text{ lbs (double sensitivity)}$$

$$P_7 = 29 * 10^6 * \left(\frac{3,445 - 3,312}{2}\right) * 10^{-6} * 0.19635 = 379 \text{ lbs}$$

$$P_6 = 29 * 10^6 * \left(\frac{706 - 582}{2}\right) * 10^{-6} * 0.19635 = 353 \text{ lbs}$$

$$P_{22} = 29 * 10^6 * \left(\frac{21,098 - 21,070}{2}\right) * 10^{-6} * 0.19635 = 159 \text{ lbs}$$

$$P_{10} = 29 * 10^6 * \left(\frac{30,170 - 30,095}{2}\right) * 10^{-6} * 0.19635 = 214 \text{ lbs}$$

Dividing these values with the area of the pressure face of the box gives the stresses (Table 7).

Table 7. Readings and Soil Stresses

Box	Initial Reading (10^{-6} in)	Final Reading (10^{-6} in)	Pressure at Rod (lbs)	Soil Stress (lbs/sq in)	Initial Soil Stresses (lbs/sq in)	Total Soil Stresses (lbs/sq in)
8	4,482	4,580	279	10.7	7.3	18.0
7	3,312	3,445	379	13.7	7.3	20.8
6	582	706	353	14.6	7.3	21.9
22	21,070	21,098	159	6.2	0.2	6.4
10	30,095	30,170	214	8.2	2.1	10.3

Note: The readings were from load increment 5 (Table 3).

The soil stress at box 8 should have been greater than the stress at box 6; the stress at box 22 was also expected to be greater than that at box 10 as the foundation was rotating to the left (Fig. 31). The rest of the data also showed that the computed soil stresses (according to the readings) were not usable.

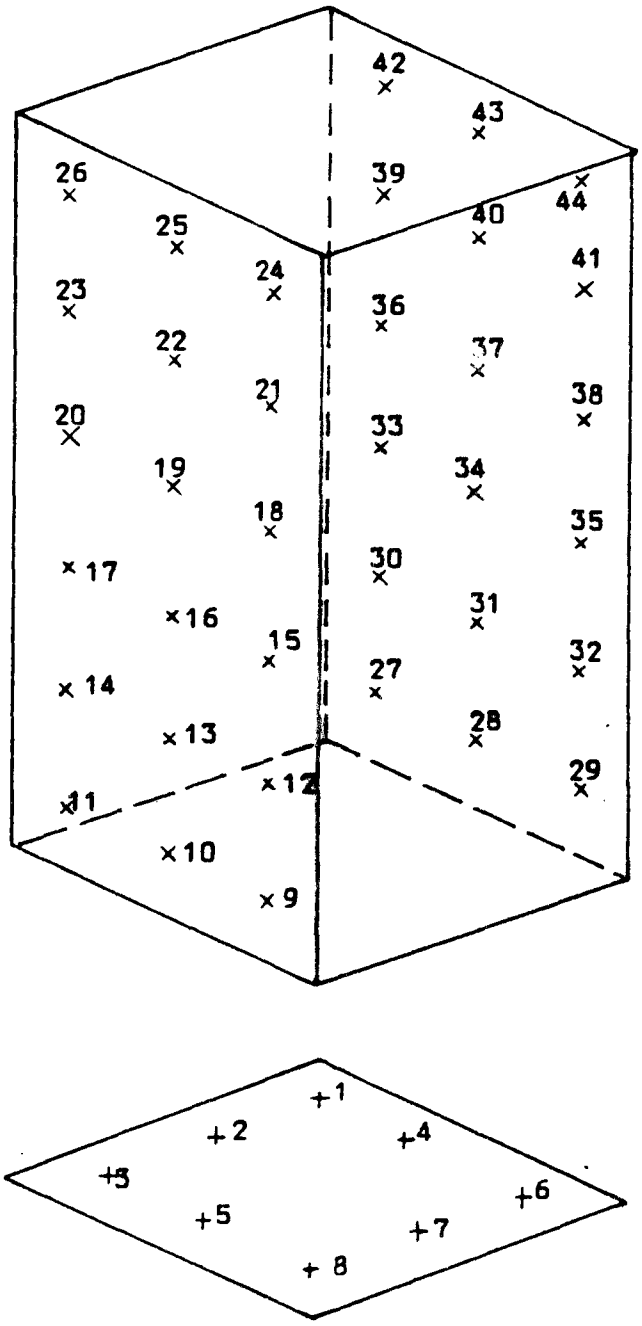

Figure 31 Location of Strain Gage Boxes at the Foundation

APPENDIX D

DETERMINATION OF YIELD STRESSES

The yield stresses were calculated based on Rankine's theory for passive soil pressures (having a linear pressure distribution [Fig. 32]).

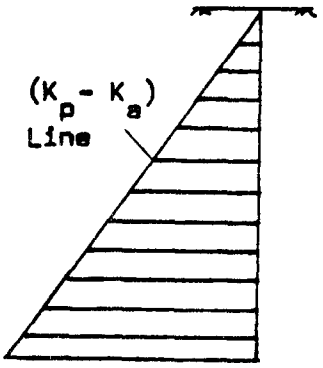

Figure 32. Linear Pressure Distribution

The passive soil pressure based on Rankine's theory for cohesionless soils is:

For sand,

$$P_p = \gamma y \tan^2(45 + \tfrac{\phi}{2}) = \gamma y K_p$$

For $\phi = 45°$ and $\gamma = 94.5$ lb/ft^3 = 0.0547 lb/in^3

$$P_p = 0.0547y(5.8284)$$

$$P_p = 0.31874y$$

For loess,

$$P_p = \gamma y \tan^2(45 + \tfrac{\phi}{2}) = \gamma y K_p \qquad (21a)$$

For $\gamma = 113$ lbs/ft^3 = 0.0654 lbs/in^3, and $\phi = 28°$ (20)

$$P_p = 0.18113y$$

For practical reasons (computer run time) the soil at the front and at the rear of the 7 ft high block foundation was divided into 7 strata, each stratum having a constant yield stress equal to the average yield stress at the middle of the stratum (Fig. 33).

For clay:

$$\sigma_y = (0.18113y)\ lb/in^2$$

Stratum 1: $\sigma_{y1} = .18113(6) = 1.091bs/in^2$

Stratum 2: $\sigma_{y2} = .18113(18) = 3.26\ lbs/in^2$

Stratum 3: $\sigma_{y3} = .18113(30) = 5.43\ lbs/in^2$

Stratum 4: $\sigma_{y4} = .18113(42) = 7.61\ lbs/in^2$

Stratum 5: $\sigma_{y5} = .18113(54) = 9.78\ lbs/in^2$

Stratum 6: $\sigma_{y6} = .18113(66) = 11.95\ lbs/in^2$

Stratum 7: $\sigma_{y7} = .18113(78) = 14.13\ lbs/in^2$

For sand:

$$\sigma_y = 0.31874y$$

Thus:

$$\sigma_{y8} = 1.91\ lbs/in^2$$

$$\sigma_{y9} = 5.73\ lbs/in^2$$

$$\sigma_{y19} = 9.56\ lbs/in^2$$

$$\sigma_{y11} = 13.38\ lbs/in^2$$

$$\sigma_{y12} = 17.2\ lbs/in^2$$

$$\sigma_{y13} = 21.04\ lbs/in^2$$

$$\sigma_{y14} = 24.86\ lbs/in^2$$

Each stratum was subdivided into three layers, all three layers having the same yield stress.

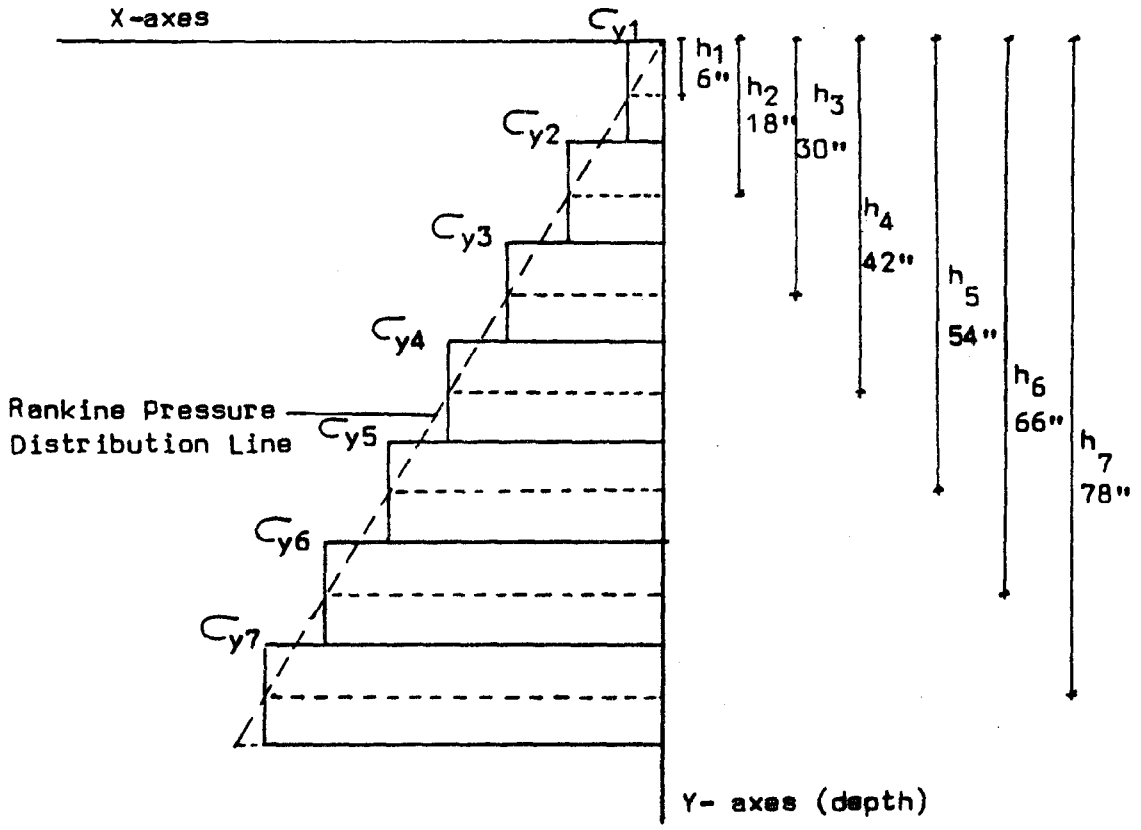

Figure 33. Average Soil Pressures Based on Rankine's Theory

Note: At the ultimate moment capacity, the results showed the location of the rotation center of the block foundation to be at a depth of about 4.89 ft from the ground surface.

The subdivision of each layer was needed for practical reasons and to lessen the effect that two layers with different yield stresses have on each other. Two adjacent layers influence each other, and if the yield stresses of those layers are different, the yield stresses of both are affected.

APPENDIX E

ANSYS INPUT AND FINAL RESULTS

```
ANSYS
/INT
/PREP7
/TITLE, MOMENT RESISTANCE OF SIDE BEARING BLOCK FOUNDATIONS
C*** THIS IS FOR BASE CORNERS,EACH CONNECTED BY 1 VERTICAL INTERF. EL.
C***  YIELD IS TAKEN INTO CONSIDERATION
C*** ELEM. NEAR CONCR. SIDES ARE 1/3 FT HIGH
      KAN,0
      ET,1,42,,,3
      ET,2,12,,,1,,,0
      ET,3,12,,,1,,,2
      ET,4,42,,,3
      KRF,1     *PRINT NODALAND REACTION FORCES
      KNL,1       *PROCESS PLASTICITY EFFECTS
      TREF,100
C*** TYPE IN THE MATERIAL PROPERTIES
      EX,15,2.2E3  *LOESS
      EX,16,10E3  *SAND
      EX,17,36E5  *CONCRETE
      NUXY,15,25E-2
      NUXY,16,35E-2
      NUXY,17,17E-2
C*** E AND NUXY FOR ORTH. ELEM.:
      EX,19,.001 $EY,19,10E3  *SAND
      EX,20,.001  *SAND
      EX,21,10E3  $EY,21,.001     *SAND
      NUXY,19,0.0
      NUXY,20,0.0
      NUXY,21,0.0
      EX,22,.001 $EY,22,2.2E3  *LOESS
      EX,23,.001  *LOESS
      EX,24,2.2E3  $EY,24,.001     *LOESS
      NUXY,22,0.0
      NUXY,23,0.0
      NUXY,24,0.0
      ACEL,0,386.4
C*** FOR LOESS (1/8 DENS.)
      DENS,1,.021E-3
      ,2,.021E-3
      ,3,.021E-3
      ,4,.021E-3
      ,5,.021E-3
      ,6,.021E-3
      ,7,.021E-3
      ,15,.021E-3
     ,22,.021E-3
     ,23,0
     ,24,0
C*** FOR SAND
      DENS,8,.018E-3
      ,9,.018E-3
      ,10,.018E-3
      ,11,.018E-3
      ,12,.018E-3
      ,13,.018E-3
      ,14,.018E-3
      DENS,16,.018E-3
      ,19,.018E-3
```

```
      ,20,0
      ,21,0
C*** FOR CONCRETE
      DENS,17,.03E-3
C*** INPUT FOR YIELD PROPERTIES
      MPTGEN,1,2,100,50
C*** ELAST. MODUL. FOR ELASTIC PORTION OF LOESS AND SAND
      MPDATA,EX,1,1,2.2E3,2.2E3
      ,EX,2,1,2.2E3,2.2E3
      ,EX,3,1,2.2E3,2.2E3
      ,EX,4,1,2.2E3,2.2E3
      ,EX,5,1,2.2E3,2.2E3
      ,EX,6,1,2.2E3,2.2E3
      ,EX,7,1,2.2E3,2.2E3
      MPDATA,EX,8,1,10E3,10E3
      ,EX,9,1,10E3,10E3
      ,EX,10,1,10E3,10E3
      ,EX,11,1,10E3,10E3
      ,EX,12,1,10E3,10E3
      ,EX,13,1,10E3,10E3
      ,EX,14,1,10E3,10E3
      MPDATA,NUXY,1,2,25E-2
  ,NUXY,2,2,25E-2
  ,NUXY,4,2,25E-2
  ,NUXY,5,2,25E-2
  ,NUXY,6,2,25E-2
  ,NUXY,7,2,25E-2
      MPDATA,NUXY,8,2,35E-2
  ,NUXY,9,2,35E-2
  ,NUXY,10,2,35E-2
  ,NUXY,11,2,35E-2
  ,NUXY,12,2,35E-2
  ,NUXY,13,2,35E-2
  ,NUXY,14,2,35E-2
      NL,1,13,2  $NL,2,13,2  $NL,3,13,2  $NL,4,13,2
      NL,5,13,2  $NL,6,13,2  $NL,7,13,2  $NL,8,13,2
      NL,9,13,2  $NL,10,13,2  $NL,11,13,2  $NL,12,13,2
      NL,13,13,2  $NL,14,13,2
      NL,1,19,100,150 $NL,2,19,100,150 $NL,3,19,100,150 $NL,4,19,100,150
      NL,5,19,100,150 $NL,6,19,100,150 $NL,7,19,100,150 $NL,8,19,100,150
      NL,9,19,100,150 $NL,10,19,100,150 $NL,11,19,100,150 $NL,12,19,100,150
      NL,13,19,100,150  $NL,14,19,100,150
      NL,1,25,1.09,1.09
      ,2,25,3.26,3.26
      ,3,25,5.43,5.43
      ,4,25,7.61,7.61
      ,5,25,9.78,9.78
      ,6,25,11.95,11.95
      ,7,25,14.13,14.13
      NL,8,25,1.82,1.82
      ,9,25,5.6,5.6
      ,10,25,9.1,9.1
      ,11,25,12.7,12.7
      ,12,25,16.4,16.4
      ,13,25,20,20
      ,14,25,23.7,23.7
C*** SLOPE OF PLASTIC PORTION
      NL,1,31,0.0001,0.0001
      ,2,31,0.0001,0.0001
      ,3,31,0.0001,0.0001
      ,4,31,0.0001,0.0001
      ,5,31,0.0001,0.0001
      ,6,31,0.0001,0.0001
      ,7,31,0.0001,0.0001
      NL,8,31,0.0001,0.0001
      ,9,31,0.0001,0.0001
```

```
      ,10,31,0.0001,0.0001
      ,11,31,0.0001,0.0001
      ,12,31,0.0001,0.0001
      ,13,31,0.0001,0.0001
      ,14,31,0.0001,0.0001
      MU,18,.4
C*** TYPE IN THE REAL CONSTANTS
C*** FOR THE CONCR. AND SOIL ELEMENTS
      R,1,1
C*** FOR CORNER SIDE INTERFACE ELEM.
      R,2,270,24E5,0,2.0
C*** FORSIDE INTERF.NODES W. STIFFNESS
      R,3,270,48E5,0,2.0
C*** FOR 0 STIFFN. SIDE INTERF.ELEM.
      R,4,270,0,-.001,2.0
C*** FOR CORNER BASE INTERF. ELEM. W. STIFFN.
      R,5,,13.5E5,0,2.0
C*** FOR BASE INTERF. ELEM. W. STIFFN.
      R,6,,27E5,0,2.0
C*** FOR CORNER INTERF.ELEM. W. 0 STIFFN.
      R,7,,0,-.001,2.0
C*** CREATE THE 409 NODES
  N,1,0,0 $N,5,96,0 $N,9,144,0 $N,11,164,0 $N,12,173.999,0 $N,13,174,0
  N,17,210,0 $N,18,210.001,0 $N,21,240,0 $N,22,252,0 $N,23,276,0
 FILL,1,5 $FILL,5,9 $FILL,9,11 $FILL,13,17 $FILL,18,21 $N,342,220,-86
  NGEN,7,45,1,23,1,,-12 $N,24,132,-4 $N,25,144,-4 $N,28,173.999,-4
 FILL,25,28 $N,29,174,-4 $NGEN,2,11,24,29,1,,-4 $N,30,210,-4 $N,31,210.001,-4
  N,34,240,-4 $FILL,31,34 $NGEN,2,11,30,34,1,,-4 $N,69,132,-16 $N,70,144,-16
  N,73,173.999,-16 $N,74,174,-16 $FILL,70,73
  NGEN,2,11,69,74,1,,-4 $N,75,210,-16 $N,76,210.001,-16 $N,79,240,-16
 FILL,76,79 $NGEN,2,11,75,79,1,,-4 $N,114,132,-28 $N,115,144,-28
  N,118,173.999,-28 $N,119,174,-28 $FILL,115,118 $NGEN,2,11,114,119,1,,-4
  N,120,210,-28 $N,121,210.001,-28 $N,124,240,-28 $FILL,121,124
  NGEN,2,11,120,124,1,,-4 $N,159,132,-40 $N,160,144,-40
  N,163,173.999,-40 $FILL,160,163 $N,164,174,-40 $NGEN,2,11,159,164,1,,-4
  N,165,210,-40 $N,166,210.001,-40 $N,169,240,-40 $FILL,166,169
  NGEN,2,11,165,169,1,,-4
  N,204,132,-52 $N,205,144,-52 $N,208,173.999,-52 $FILL,205,208 $N,209,174,-52
  NGEN,2,11,204,209,1,,-4 $N,210,210,-52 $N,211,210.001,-52 $N,214,240,-52
  FILL,211,214 $NGEN,2,11,210,214,1,,-4 $N,249,132,-64 $N,250,144,-64
  N,253,173.999,-64 $FILL,250,253 $N,254,174,-64 $NGEN,2,11,249,254,1,,-4
  N,255,210,-64 $N,256,210.001,-64 $N,259,240,-64 $FILL,256,259
  NGEN,2,11,255,259,1,,-4
  N,294,132,-76 $N,295,144,-76 $N,298,173.999,-76 $FILL,295,298
  N,299,174,-76 $NGEN,2,11,294,299,1,,-4 $N,300,210,-76 $N,301,210.001,-76
  N,304,240,-76 $FILL,301,304 $NGEN,2,11,300,304,1,,-4 $N,316,174,-84
  N,320,210,-84 $FILL,316,320 $N,321,174,-84.001 $N,325,210,-84.001
  N,326,0,-84 $N,330,96,-84 $N,333,132,-84 $FILL,321,325 $FILL,326,330
  FILL,330,333 $N,334,144,-86 $N,337,174,-86 $N,341,210,-86 $N,344,240,-86
  NGEN,2,55,271,278,1,,-12 $FILL,334,337 $FILL,337,341 $FILL,342,344
  NGEN,2,53,292,293,1,,-12 $NGEN,2,76,271,281,1,,-24 $N,358,174,-96
  N,362,210,-96 $N,365,240,-96 $N,366,252,-96 $N,367,276,-96 $FILL,358,362
  FILL,362,365 $NGEN,3,21,347,367,1,,-12
C*** CREATE THE 407 ELEMENTS :
C*** LOESS ELEM.
  TYPE,4 $REAL,1 $MAT,22 $E,46,47,2,1 $EGEN,3,1,1
 TYPE,4 $REAL,1 $MAT,24 $E,49,50,5,4
  TYPE,1 $REAL,1 $MAT,1 $E,50,51,6,5 $EGEN,2,1,4 $E,24,8,7,7
  E,52,35,24,7 $E,53,35,52,52 $E,24,25,9,8 $E,35,36,25,24 $E,53,54,36,35
  TYPE,4 $REAL,1 $MAT,24 $E,21,34,22,22 $E,45,67,22,34
  TYPE,1 $REAL,1 $MAT,1 $E,45,66,67,67 $E,67,68,23,22
  TYPE,1 $REAL,1 $MAT,2 $E,91,92,47,46 $TYPE,4 $REAL,1 $MAT,24
   E,92,93,48,47 $TYPE,1 $REAL,1 $MAT,2 $E,93,94,49,48
 TYPE,4 $REAL,1 $MAT,24 $E,94,95,50,49 $TYPE,1 $REAL,1 $MAT,2 $E,95,96,51,50
 TYPE,4 $REAL,1 $MAT,24 $E,96,97,52,51 $TYPE,1 $REAL,1 $MAT,2
  E,69,53,52,52 $E,97,80,69,52 $TYPE,4 $REAL,1 $MAT,24 $E,98,80,97,97
```

```
  TYPE,1 $REAL,1 $MAT,2 $E,69,70,54,53 $E,80,81,70,69 $E,98,99,81,80
TYPE,4 $REAL,1 $MAT,24 $E,66,79,67,67 $TYPE,4 $REAL,1 $MAT,23 $E,98,112,67,79
TYPE,4 $REAL,1 $MAT,22 $E,90,111,112,112 $TYPE,4 $REAL,1 $MAT,23
  E,112,113,68,67
  TYPE,1 $REAL,1 $MAT,3 $E,136,137,92,91 $EGEN,5,1,33 $TYPE,4 $REAL,1 $MAT,24
  E,141,142,97,96 $TYPE,1 $REAL,1 $MAT,3 $E,114,98,97,97 $E,142,125,114,97
  E,143,125,142,142 $E,114,115,99,98 $E,125,126,115,114
  E,143,144,126,125 $TYPE,4 $REAL,1 $MAT,22 $E,111,124,112,112
  E,135,157,112,124 $E,135,156,157,157
 E,157,158,113,112
  TYPE,1 $REAL,1 $MAT,4 $E,181,182,137,136 $EGEN,4,1,49
 TYPE,4 $REAL,1 $MAT,24 $E,185,186,141,140 $E,186,187,142,141
  E,159,143,142,142 $TYPE,1 $REAL,1 $MAT,4 $E,187,170,159,142
  E,188,170,187,187 $E,159,160,144,143 $E,170,171,160,159 $E,188,189,171,170
  TYPE,4 $REAL,1 $MAT,23 $E,156,169,157,157 $E,180,202,157,169
  E,188,201,202,202 $E,202,203,158,157 $TYPE,1 $REAL,1 $MAT,5
  E,226,227,182,181 $EGEN,4,1,65 $TYPE,4 $REAL,1 $MAT,24 $E,230,231,186,185
  TYPE,1 $REAL,1 $MAT,5 $E,231,232,187,186 $E,204,188,187,187
  E,232,215,204,187
  E,233,215,232,232 $E,204,205,189,188 $E,215,216,205,204 $E,233,234,216,215
 TYPE,4 $REAL,1 $MAT,23 $E,201,214,202,202 $TYPE,4 $REAL,1 $MAT,24
  E,225,247,202,214 $E,225,246,247,247 $TYPE,4 $REAL,1 $MAT,23
 E,247,248,203,202 $TYPE,1 $REAL,1 $MAT,6
E,271,272,227,226 $EGEN,3,1,81 $TYPE,4 $REAL,1 $MAT,24 $E,274,275,230,229
  TYPE,1 $REAL,1 $MAT,6 $E,275,276,231,230
  EGEN,2,1,85 $E,249,233,232,232 $E,277,260,249,232
  E,278,260,277,277 $E,249,250,234,233 $E,260,261,250,249 $E,278,279,261,260
 TYPE,4 $REAL,1 $MAT,24 $E,246,259,247,247
  E,270,292,247,259 $E,270,291,292,292 $E,292,293,248,247
      TYPE,1 $REAL,1 $MAT,7
  E,326,327,272,271 $EGEN,6,1,97 $E,294,278,277,277 $E,332,305,294,277
  E,333,305,332,332 $E,294,295,279,278 $TYPE,4 $REAL,1 $MAT,22
 E,305,306,295,294 $E,333,334,306,305 $TYPE,4 $REAL,1 $MAT,24
  E,291,304,292,292 $tYPE,4 $REAL,1 $MAT,23 $E,315,345,292,304
TYPE,4 $REAL,1 $MAT,24 $E,315,344,345,345 $E,345,346,293,292
      TYPE,1  $REAL,1  $MAT,15
 E,347,348,327,326 $EGEN,7,1,113
 TYPE,4 $REAL,1 $MAT,22 $E,354,355,334,333
 EGEN,7,1,120 $TYPE,4 $REAL,1 $MAT,23 $E,361,362,341,340
 TYPE,1 $REAL,1 $MAT,22  $E,362,363,342,341  $EGEN,2,1,120
 TYPE,1 $REAL,1 $MAT,15 $E,364,365,344,343 $EGEN,2,1,130
 TYPE,4 $REAL,1 $MAT,22 $E,366,367,346,345
TYPE,1 $REAL,1 $MAT,15 $E,368,369,348,347 $EGEN,6,1,133
 TYPE,4 $REAL,1 $MAT,22 $E,374,375,354,353 $EGEN,14,1,139
 TYPE,1 $REAL,1 $MAT,15 $E,389,390,369,368 $EGEN,5,1,153
 TYPE,4 $REAL,1 $MAT,23 $E,394,395,374,373 $EGEN,2,1,158
 TYPE,4 $REAL,1 $MAT,22
  E,396,397,376,375 $TYPE,1 $REAL,1 $MAT,15 $E,397,398,377,376
 TYPE,4 $REAL,1 $MAT,24 $E,398,399,378,377
 TYPE,4 $REAL,1 $MAT,22 $E,399,400,379,378 $EGEN,10,1,163
C*** SAND ELEM.
      TYPE,1  $REAL,1  $MAT,8
  E,25,26,10,9 $EGEN,3,1,173 $TYPE,4 $REAL,1 $MAT,21 $E,36,37,26,25
 TYPE,1 $REAL,1 $MAT,8 $E,37,38,27,26 $EGEN,2,1,177 $TYPE,4 $REAL,1 $MAT,21
 E,54,55,37,36 $TYPE,1 $REAL,1 $MAT,8 $E,55,56,38,37 $EGEN,2,1,180
  E,31,32,19,18 $EGEN,3,1,182 $E,42,43,32,31  $EGEN,2,1,185
 TYPE,4 $REAL,1 $MAT,20 $E,44,45,34,33 $TYPE,1 $REAL,1 $MAT,8
  E,63,64,43,42 $EGEN,2,1,188 $TYPE,4 $REAL,1 $MAT,20 $E,65,66,45,44
  TYPE,4  $REAL,1  $MAT,21 $E,70,71,55,54 $TYPE,1 $REAL,1 $MAT,9
 E,71,72,56,55 $EGEN,2,1,192 $TYPE,4 $REAL,1 $MAT,21
  E,81,82,71,70 $TYPE,1 $REAL,1 $MAT,9 $E,82,83,72,71 $EGEN,2,1,195
TYPE,4 $REAL,1 $MAT,21 $E,99,100,82,81 $TYPE,1 $REAL,1 $MAT,9 $E,100,101,83,82
  EGEN,2,1,198 $E,76,77,64,63
 TYPE,4 $REAL,1 $MAT,19 $E,77,78,65,64 $TYPE,1 $REAL,1 $MAT,9 $E,78,79,66,65
  E,87,88,77,76  $E,88,89,78,77 $EGEN,2,1,204 $TYPE,4 $REAL,1 $MAT,19
  E,108,109,88,87 $E,109,110,89,88 $EGEN,2,1,207
   TYPE,4  $REAL,1  $MAT,21 $E,115,116,100,99 $TYPE,1 $REAL,1 $MAT,10
```

```
   E,116,117,101,100 $EGEN,2,1,210 $E,126,127,116,115 $EGEN,3,1,212
   E,144,145,127,126 $EGEN,3,1,215 $TYPE,4 $REAL,1 $MAT,19
   E,121,122,109,108 $EGEN,3,1,218 $E,132,133,122,121 $EGEN,3,1,221
 TYPE,1 $REAL,1 $MAT,10 $E,153,154,133,132 $TYPE,4 $REAL,1 $MAT,20
   E,154,155,134,133
    TYPE,4 $REAL,1 $MAT,19 $E,155,156,135,134 $TYPE,1  $REAL,1  $MAT,11
   E,160,161,145,144 $EGEN,3,1,227 $E,171,172,161,160 $EGEN,3,1,230
   E,189,190,172,171 $EGEN,3,1,233 $E,166,167,154,153 $EGEN,2,1,236
 TYPE,4 $REAL,1 $MAT,21 $E,168,169,156,155 $TYPE,4 $REAL,1 $MAT,20
   E,177,178,167,166
  EGEN,2,1,239 $TYPE,4 $REAL,1 $MAT,20 $E,179,180,169,168 $TYPE,1 $REAL,1 $MAT,11
   E,198,199,178,177 $TYPE,4 $REAL,1 $MAT,20 $E,199,200,179,178
   TYPE,4 $REAL,1 $MAT,19 $E,200,201,180,179 $TYPE,1  $REAL,1  $MAT,12
     E,205,206,190,189 $EGEN,3,1,245 $E,216,217,206,205 $EGEN,3,1,248
  E,234,235,217,216 $EGEN,2,1,251 $TYPE,4 $REAL,1 $MAT,19 $E,236,237,219,218
   E,211,212,199,198 $TYPE,4 $REAL,1 $MAT,20 $E,212,213,200,199
   E,213,214,201,200 $TYPE,4 $REAL,1 $MAT,20 $E,222,223,212,211
  TYPE,4 $REAL,1 $MAT,21 $E,223,224,213,212 $E,224,225,214,213
  TYPE,4 $REAL,1 $MAT,20
   E,243,244,223,222 $E,244,245,224,223 $TYPE,1 $REAL,1 $MAT,13
   E,245,246,225,225  $E,250,251,235,234
  TYPE,4 $REAL,1 $MAT,21 $E,251,252,236,235 $TYPE,4 $REAL,1 $MAT,19
 E,252,253,237,236 $TYPE,1 $REAL,1 $MAT,13 $E,261,262,251,250
  TYPE,4 $REAL,1 $MAT,21 $E,262,263,252,251 $TYPE,4 $REAL,1 $MAT,20
  E,263,264,253,252 $TYPE,4 $REAL,1 $MAT,19
   E,279,280,262,261 $TYPE,4 $REAL,1 $MAT,20 $E,280,281,263,262 $EGEN,2,1,270
 TYPE,4 $REAL,1 $MAT,21 $E,256,257,244,243 $EGEN,2,1,272
  TYPE,4 $REAL,1 $MAT,20
 E,258,259,246,245 $TYPE,4 $REAL,1 $MAT,21 $E,267,268,257,256 $EGEN,2,1,275
  E,269,270,259,258 $TYPE,1 $REAL,1 $MAT,13
  E,288,289,268,267 $TYPE,4 $REAL,1 $MAT,21 $E,289,290,269,268
   TYPE,1 $REAL,1 $MAT,13 $E,290,291,270,269
  TYPE,4 $REAL,1 $MAT,19 $E,295,296,280,279 $TYPE,4 $REAL,1 $MAT,20
  E,296,297,281,280 $EGEN,2,1,282 $TYPE,4 $REAL,1 $MAT,19
  E,306,307,296,295 $TYPE,4 $REAL,1 $MAT,20 $E,307,308,297,296
  EGEN,2,1,285 $TYPE,4 $REAL,1 $MAT,19 $E,334,335,307,306
  TYPE,4 $REAL,1 $MAT,20
  E,335,336,308,307 $E,336,321,309,308 $TYPE,1 $REAL,1 $MAT,14
  E,301,302,289,288 $TYPE,4 $REAL,1 $MAT,21 $E,302,303,290,289
  E,303,304,291,290 $TYPE,1 $REAL,1 $MAT,14 $E,312,313,302,301
  TYPE,4 $REAL,1 $MAT,20 $E,313,314,303,302 $EGEN,2,1,294
   TYPE,1 $REAL,1 $MAT,14 $E,325,342,313,312 $TYPE,4 $REAL,1 $MAT,21
 E,342,343,314,313 $E,343,344,315,314 $TYPE,4 $REAL,1 $MAT,19
  E,337,321,336,336 $E,337,338,322,321 $EGEN,3,1,300 $TYPE,4 $REAL,1 $MAT,20
  E,340,341,325,324 $E,325,341,342,342
 C*** CONCRETE $ELEM.
       TYPE,1  $REAL,1  $MAT,17
   E,13,29,14,14 $E,40,59,14,29 $E,40,58,59,59 $E,59,60,15,14 $EGEN,2,1,308
   E,30,17,16,16 $E,61,41,30,16 $E,62,41,61,61 $E,58,74,59,59 $E,85,104,59,74
   E,85,103,104,104
   E,104,105,60,59 $EGEN,2,1,316 $E,75,62,61,61 $E,106,86,75,61
   E,107,86,106,106 $E,103,119,104,104 $E,130,149,104,119 $E,130,148,149,149
   E,149,150,105,104 $EGEN,2,1,324 $E,120,107,106,106 $E,151,131,120,106
   E,151,152,131,131
   E,148,164,149,149 $E,175,194,149,164 $E,175,193,194,194 $E,194,195,150,149
   EGEN,2,1,332 $E,165,152,151,151 $E,196,176,165,151 $E,197,176,196,196
   E,193,209,194,194 $E,220,239,194,209 $E,220,238,239,239 $E,239,240,195,194
   EGEN,2,1,340 $E,210,197,196,196 $E,241,221,210,196
   E,242,221,241,241   $E,238,254,239,239
   E,265,284,239,254 $E,265,283,284,284 $E,284,285,240,239 $EGEN,2,1,348
   E,255,242,241,241 $E,286,266,255,241 $E,287,266,286,286
   E,283,299,284,284 $E,310,317,284,299 $E,310,316,317,317 $E,317,318,285,284
   EGEN,2,1,356 $E,300,287,286,286 $E,286,319,311,300 $E,320,311,319,319
 C*** INTERFACE ELEM.
 C*** CORNERS HAVE DIFFERENT STIFFNESSES
       TYPE,2  $REAL,2  $MAT,18  $E,12,13
       TYPE,2  $REAL,3  $MAT,18  $E,28,29  $EGEN,2,11,362 $E,57,58 $E,73,74
```

```
      EGEN,2,11,365 $E,102,103 $E,118,119 $EGEN,2,11,368 $E,147,148
      E,163,164 $EGEN,2,11,371 $E,192,193
      $TYPE,3 $REAL,4 $MAT,18 $E,208,209 $E,219,220 $E,237,238
      E,253,254 $EGEN,2,11,377 $E,282,283 $E,298,299 $EGEN,2,11,380
      TYPE,3  $REAL,4  $MAT,18  $E,17,18  $E,30,31 $EGEN,2,11,383 $E,62,63
      E,75,76 $EGEN,2,11,386 $E,107,108 $E,120,121 $EGEN,2,11,389
      E,152,153 $E,165,166 $EGEN,2,11,392 $E,197,198 $E,210,211
      EGEN,2,11,395
      TYPE,2 $REAL,3 $MAT,18 $E,242,243 $E,255,256
      E,266,267 $E,287,288 $E,300,301 $EGEN,2,11,401
      TYPE,2  $REAL,5  $MAT,18  $E,321,316
      TYPE,2  $REAL,6  $MAT,18  $E,322,317 $E,323,318
      TYPE,3  $REAL,7  $MAT,18  $E,324,319 $EGEN,2,1,406
C*** 1ST LOAD STEP
      ITER,-5,1,1
      TUNIF,100.0
      CNVR,.03,,.01,,0
C***  DETERMINE THE BOUNDARY CONDITIONS
      D,1,UX,0,,271,45  $D,326,UX,0,,368,21  $D,389,UX,0,,409,1,UY
      D,23,UX,0,,293,45  $D,346,UX,0,,388,21
      F,369,FY,-.01
LWRITE
AFWRITE
FINISH
/EXE313
/INPUT,27
FINISH
/POST1
FINISH
/EOF
ANSYS
/INT
/PREP7
RESUME
--
--
--
      DENS,1,.1695E-3
      ,2,.1695E-3
      ,3,.1695E-3
      ,4,.1695E-3
      ,5,.1695E-3
      ,6,.1695E-3
      ,7,.1695E-3
      ,15,.1695E-3
      ,22,.1695E-3
      ,23,.1695E-3
      ,24,.1695E-3
C*** FOR SAND
      DENS,8,.1415E-3
      ,9,.1415E-3
      ,10,.1415E-3
      ,11,.1415E-3
      ,12,.1415E-3
      ,13,.1415E-3
      ,14,.1415E-3
      DENS,16,.1415E-3
      ,19,.1415E-3
      ,20,.1415E-3
      ,21,.1415E-3
C*** FOR CONCRETE
      DENS,17,.2252E-3
C*** 8TH LOAD STEP
      ITER,-3,1,1
      TUNIF,100.0
      CNVR,.03,,.01,,0
C***  DETERMINE THE BOUNDARY CONDITIONS
      D,1,UX,0,,271,45  $D,326,UX,0,,368,21  $D,389,UX,0,,409,1,UY
```

```
      D,23,UX,0,,293,45  $D,346,UX,0,,388,21
      F,15,FY,-49.5  $F,14,FY,-289  $F,16,FY,289  $F,15,FX,-19.3
LWRITE
--
--
--
C*** 115TH LOAD STEP
      ITER,-4,1,1
      TUNIF,100.0
      CNVR,.03,,.01,,0
      F,15,FY,-266  $F,14,FY,-1572  $F,16,FY,1572  $F,15,FX,-111.9
LWRITE
SLOAD,1
AFWRITE
FINISH
/LOAD
/INPUT,27
FINISH
/POST1
STRESS,FX,42,1
STRESS,FY,42,2
SET,115,3  $NLINES,4000  $PRSTRES
EALL $NLINES,1000 $ESEL,ELEM,361,407 $PREFOR
EALL  $NLINES,2000  $NRSEL,NODE,13,320  $PRDISP
EALL $NLINES,2000 $ESEL,ELEM,299,304 $PRESTR
EALL $NLINES,2000 $ESEL,ELEM,122,129 $PRESTR
FINISH
/EOF
COMO -END
LO
```

SAMPLE OUTPUT FOR SOIL ELEMENT STRESSES (ELEMENTS ADJACENT TO THE INTERFACE ELEMENTS, AT THE SIDE BEARING WALLS).

```
        ***** POST1 ELEMENT STRESS LISTING *****

 LOAD STEP   115  ITERATION=     3  SECTION=  1

  ELEM      FX          FY
C** FOR ELEMENTS AT THE FRONT FACE, ADJACENT TO
THE INTERFACE ELEMENTS:
  175   -2.7404      -2.3147
  178   -2.6756      -2.2317
  181   -2.4369      -2.3083
  193   -6.5021      -4.5136
  196   -6.3914      -4.4464
  199   -6.8283      -4.5315
  211   -10.338      -4.4445
  214   -9.8984      -5.2448
  217   -11.618      -6.3588
  229   -13.538      -7.3890
  232   -11.410      -7.3908
  235   -8.3712      -6.3716
  247   -10.885      -4.8127
  250   -5.4487      -2.1891
  253  -0.29002E-05-0.23471
  265  -0.51064E-05 0.14314E-01
  268   0.11818E-04 0.30758E-05
  271   0.83034E-05 0.87548E-05
  283   0.12609E-04 0.22385E-04
  286   0.37393E-04 0.43160E-04
  289   0.13115E-03 0.56888E-04
C** FOR ELEMENTS AT THE REAR FACE, ADJACENT TO
THE INTERFACE ELEMENTS:
  182  -0.13415     -0.43971E-01
  185   0.56896E-01-0.12661
  188  -0.21381     -0.21031
  200  -0.13625     -0.24162
  203  -0.11380E-01-0.21980
  206  -0.19910E-03-0.21743
  218  -0.74939E-03-0.25002
  221  -0.55027E-03-0.28246
  224   0.20083E-01-0.44135
  236  -0.31772E-01-0.32655
  239  -0.77638E-08-0.37696
  242  -0.13095E-01-0.55549
  254  -0.27644E-02-0.54918
  257  -0.23117E-01-0.46795
  260  -0.20353E-01-0.46662
  272   -4.1638     -0.18961
  275   -26.979     -0.17992
  278   -16.978      0.06977
  290   -8.9427      0.00676
  293   -13.686      0.05853
  296   -10.504      0.08344
```

APPENDIX F

DESIGN OF SIDE BEARING BLOCK FOUNDATIONS

For the design of side bearing block foundations, decisive limits are needed,

A) The design loads, obtained by multiplying the loads acting on the foundation (obtained by applying the factored loads to the superstructure) by safety factors.

B) The allowable rotation.

The functional requirements of the superstructure determine the magnitude of the safety factors. The design loads (used to obtain the dimensions of the foundation from the design equations) are obtained by multiplying the allowable loads by safety factors. The allowable loads for the foundation are obtained by applying the factored loads (from building codes) to the superstructure.

Each structure will have its own specifications for the magnitudes of total and differential settlements, rotation, etc. The magnitudes of the safety factors are determined by those specifications. In the following, a general case is discussed where the bearing capacity and an allowable rotation of .0025 rad (38) are the only two determining specified factors.

Design loads. Different safety factors are suggested for the overturning loads (moment and horizontal force) and the vertical load. For a square footing and a ratio of $\frac{L}{B} = \frac{7}{3}$ (Section 6), a safety factor of 6 is suggested for the moment and horizontal load for cohesionless soils (Fellenius [16] used a safety factor of 5 for laterally loaded piles in cohesive soils). The suggested safety factor for the vertical load is 2

for cohesionless soils, in accordance with usual practice for concentric vertical loads. These safety factors will be applied to Equations 3.2a to 3.8a (Section 3.5). These design equations are based on the assumption that the lateral earth pressures at the ultimate soil resistance are 2½ times the earth pressures based on Rankine's theory. Equations 3.2a to 3.8a are used (Section 3.5).

Allowable rotation. The magnitude of the allowable rotation depends on the functional requirements of the structure. A rotation of 0.0025 rad. is generally allowed (38).

Foundation design. The procedure is as follows:

1) The dimensions of the block foundation are computed using the design loads.
2) The rotation is then computed by applying the allowable loads to the foundation. The calculated rotation should be smaller than the allowable rotation.

The following data are known:

The allowable loads are

$H = -1830$ lbs

$M = -20{,}215$ lb-ft (at the top of the foundation)

$\mu = 0.57$

$V = -9{,}555$ lbs

$\phi = 45°$ (sand backfill)

$\phi = 28°$ (soil at the base of the foundation)

$\gamma = 119$ lbs/cu ft (sand)

$c = 0$

n_h = 56 ton/cu ft = 112,000 lbs/cu ft
(coefficient of horizontal subgrade reaction [5])

1. Computation of the dimensions: The design loads are obtained by using a safety factor of 6 for the lateral load and moment and a safety factor of 2 for the vertical load.

$H_D = 6 * H = -10{,}980$ lbs

$M_D = 6 * M = -121{,}290$ lb-ft ($M_u = M_D - H_D * 7 = 198{,}150$ lb-ft)

$V = 2 * 9{,}555 = 19{,}110$ lbs

assume B = 3 ft and L = 7 ft (Fig. 15)

Using Equation 3.6a (Section 3.5) $Y_{rc} = 5.47$ ft

Using Equation 3.7a, $Y_3 = 0.735$ ft

$\sigma_{bc} = 21{,}480$ psf (Appendix A)

Using Equation 3.5a (Section 3.5) $X_{rc} = 0.593$ ft

Using Equation 3.8a, D = 3 ft

The dimensions are: L = 7 ft

B = 3 ft

D = 3 ft

2. Rotation:

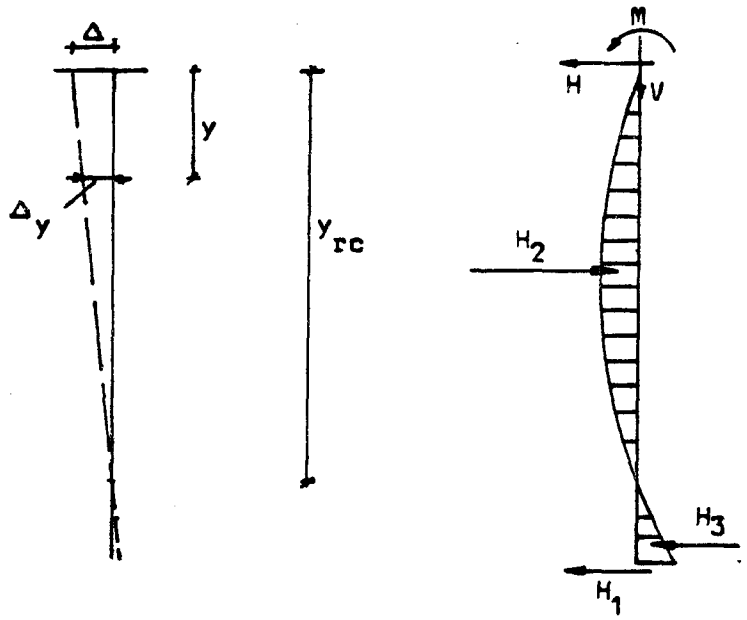

Figure 34. Soil Pressure Diagram of the Block Foundation

To compute the rotation, the "rigid pile theory" is adopted here and applied to the block foundation. The additional moment resistance due to the vertical soil reaction at the base is neglected; the error in the computed rotation is an error on the safe side.

$$H_{1,max} = 0.57 * 9,555 = -5,446 \text{ lbs}$$

The deflection at the top is assumed to be Δ. The deflection Δ_y at depth Y (Fig. 34) is:

$$\Delta_y = \frac{Y_{rc} - y}{Y_{rc}} \Delta$$

The pressure at depth y at the foundation is: $P_y = B K_s \Delta_y$

$$P_y = B(n_h \frac{y}{B})\Delta_y = n_h(\frac{yY_{rc} - y^2}{Y_{rc}})\Delta$$

$$H_2 + H_3 = \int_0^L P_y dy = \frac{n_h}{Y_{rc}}\left(\frac{Y_{rc}L^2}{2} - \frac{L^3}{3}\right)\Delta$$

$\Sigma H = 0$ gives:

$$\Delta \frac{n_h}{Y_{rc}}\left(\frac{Y_{rc}L^2}{2} - \frac{L^3}{3}\right) = H_{1,max} + H = -7,276 \qquad (a)$$

The resisting moment (of the soil) M_{res} (about the groundline):

$$M_{res} = \frac{n_h \Delta}{Y_{rc}} \int_0^L (yY_{rc} - y^2)\, ydy = \frac{n_h}{Y_{rc}} \left(\frac{Y_{rc}L^3}{3} - \frac{L^4}{4}\right)\Delta$$

Taking moments about the ground level gives:

$$\Delta \frac{n_h}{Y_{rc}}\left(\frac{Y_{rc}L^3}{3} - \frac{L^4}{4}\right) = H_{1,max} * L - M = -17,604 \qquad (b)$$

dividing (b) with (a) gives:

$$Y_{rc} = 5.88 \text{ ft}$$

substituting Y_{rc} in equation (b) gives:

$$\Delta = .01283 \text{ ft, and the rotation}$$

$$\alpha = \frac{.01283}{Y_{rc}} = 0.0022 \text{ rad.} < \text{allowable rotation } (.0025)$$

O.K.: The dimensions can be maintained.

Note: The horizontal deflection Δ, calculated with this method will be compared with the deflection h obtained from the field test for load increment 3 and 5 (Table 4).

a. For load increment 3, H = -1,310 lbs; V = -17,120 lbs; M = -54,710 lb-ft, acting at the center of the base of the foundation. The moment acting at the top is therefore

$$M = -54,710 - (-1,310 * 7) = -45,540 \text{ lb-ft}$$

$$H_{1,max} = -17,120 * 0.57 = -9,758 \text{ lbs}$$

as before

$$\Delta \frac{n_h}{Y_{rc}} \left(\frac{Y_{rc} L^2}{2} - \frac{L^3}{3} \right) = H_{1,max} + H = -11,068 \qquad (a)$$

$$\Delta \frac{n_h}{Y_{rc}} \left(\frac{Y_{rc} L^2}{3} - \frac{L^4}{4} \right) = H_{1,max} * L - M = -22,766 \qquad (b)$$

dividing (b) by (a) gives:

$Y_{rc} = 5.71$ ft

$\Delta_{total} = .0221$ ft = 6.7 mm

The deflection Δ for the "static" loads (H = -1,310 lbs; V = -3,110; M = -23,490), calculated as before is

$H_{1,max} = -3,110 * 0.57 = -1,773$ lbs

$\Delta_{stat} = .0173$ ft = 5.27 mm

Δ for load increment 3 is

$\Delta = \Delta_{tot} - \Delta_{stat} = 1.43$ mm

The field test showed for load increment 3:

h = 1.386 mm.

b. For load increment 5, H = -3,310 lbs; V = -20,310 lbs; M_o = -104,970 lbs. The moment at the top is

$M = -104,970 - (-3,310 * 7) = -81,800$ lb-ft

$H_{1,max} = -20,310 * 0.57 = 11,576$ lbs

$\Delta_{tot} = 0.05244$ ft = 15.98 mm

Δ for load increment 5 is

$\Delta = \Delta_{tot} - \Delta_{stat} = 15.98 - 5.27 = 10.71$ mm

The field test showed for load increment 5:

h = 11.086 mm.

Note: For cohesive soils, the modulus of subgrade reaction can be assumed to be $K_s = \frac{50c}{B}$ (16), where c is the undrained shear strength of the clay.